NASA/TM–2017-219601
ARL-RP-0592

A Dynamic Calibration Method for Experimental and Analytical Hub Load Comparison

Andrew R. Kreshock, Robert P. Thornburgh, and Matthew L. Wilbur
U.S. Army Research Laboratory
Vehicle Technology Directorate
Langley Research Center, Hampton, Virginia

March 2017

NASA STI Program . . . in Profile

Since its founding, NASA has been dedicated to the advancement of aeronautics and space science. The NASA scientific and technical information (STI) program plays a key part in helping NASA maintain this important role.

The NASA STI program operates under the auspices of the Agency Chief Information Officer. It collects, organizes, provides for archiving, and disseminates NASA's STI. The NASA STI program provides access to the NTRS Registered and its public interface, the NASA Technical Reports Server, thus providing one of the largest collections of aeronautical and space science STI in the world. Results are published in both non-NASA channels and by NASA in the NASA STI Report Series, which includes the following report types:

- TECHNICAL PUBLICATION. Reports of completed research or a major significant phase of research that present the results of NASA Programs and include extensive data or theoretical analysis. Includes compilations of significant scientific and technical data and information deemed to be of continuing reference value. NASA counter-part of peer-reviewed formal professional papers but has less stringent limitations on manuscript length and extent of graphic presentations.

- TECHNICAL MEMORANDUM. Scientific and technical findings that are preliminary or of specialized interest, e.g., quick release reports, working papers, and bibliographies that contain minimal annotation. Does not contain extensive analysis.

- CONTRACTOR REPORT. Scientific and technical findings by NASA-sponsored contractors and grantees.

- CONFERENCE PUBLICATION. Collected papers from scientific and technical conferences, symposia, seminars, or other meetings sponsored or co-sponsored by NASA.

- SPECIAL PUBLICATION. Scientific, technical, or historical information from NASA programs, projects, and missions, often concerned with subjects having substantial public interest.

- TECHNICAL TRANSLATION. English-language translations of foreign scientific and technical material pertinent to NASA's mission.

Specialized services also include organizing and publishing research results, distributing specialized research announcements and feeds, providing information desk and personal search support, and enabling data exchange services.

For more information about the NASA STI program, see the following:

- Access the NASA STI program home page at http://www.sti.nasa.gov

- E-mail your question to help@sti.nasa.gov

- Phone the NASA STI Information Desk at 757-864-9658

- Write to:
  NASA STI Information Desk
  Mail Stop 148
  NASA Langley Research Center
  Hampton, VA 23681-2199

NASA/TM–2017-219601
ARL-RP-0592

A Dynamic Calibration Method for Experimental and Analytical Hub Load Comparison

Andrew R. Kreshock, Robert P. Thornburgh, and Matthew L. Wilbur
U.S. Army Research Laboratory
Vehicle Technology Directorate
Langley Research Center, Hampton, Virginia

National Aeronautics and
Space Administration

Langley Research Center
Hampton, Virginia 23681-2199

March 2017

Available from:

NASA STI Program / Mail Stop 148
NASA Langley Research Center
Hampton, VA 23681-2199
Fax: 757-864-6500

ABSTRACT

This paper presents the results from an ongoing effort to produce improved correlation between analytical hub force and moment prediction and those measured during wind-tunnel testing on the Aeroelastic Rotor Experimental System (ARES), a conventional rotor testbed commonly used at the Langley Transonic Dynamics Tunnel (TDT). A frequency-dependent transformation between loads at the rotor hub and outputs of the testbed balance is produced from frequency response functions measured during vibration testing of the system. The resulting transformation is used as a dynamic calibration of the balance to transform hub loads predicted by comprehensive analysis into predicted balance outputs. In addition to detailing the transformation process, this paper also presents a set of wind-tunnel test cases, with comparisons between the measured balance outputs and transformed predictions from the comprehensive analysis code CAMRAD II. The modal response of the testbed is discussed and compared to a detailed finite-element model. Results reveal that the modal response of the testbed exhibits a number of characteristics that make accurate dynamic balance predictions challenging, even with the use of the balance transformation.

INTRODUCTION

As a result of the rising costs for wind-tunnel testing of rotor systems, achieving quality experimental data for comparison with analysis has become a critical component in the effort to validate comprehensive modeling techniques. Traditionally, the measurement of dynamic rotor loads transmitted to the fixed-system has been a significant challenge, and correlations between predicted loads and measured loads have historically produced mediocre results. Modern rotor system testbeds have strain-gauge balances that are typically used to measure the load transmitted from the rotating system to the fixed system during wind-tunnel testing. This technique has a number of drawbacks that result in differences between the balance output and the loads at the hub. First, due to imperfections in manufacturing and applying strain gauges to the balance, individual output channels tend to be coupled to each other. Thus, a single force applied to the balance most often results in outputs on all six channels of the balance. This is typically compensated for by performing a static calibration of the balance to develop a transformation matrix that can be used to "back out" the applied forces and moments. Second, contrary to its stated intention, a balance does not actually measure forces and moments, but instead measures the strain at the various flexures in the balance. When loaded statically, these strains are easily converted into forces and moments using calibration data. In a dynamic system, however, these strains are induced not only by external loads, but also by the dynamic response of the entire testbed. Further complicating matters is the fact that the balance flexures are often flexurally soft relative to the rest of the system, and thus, contribute to system resonances that can result in large balance outputs for relatively small loads. Finally, the balance loads are not only induced by the rotor hub loads, but also by loads transmitted via the pitch links to the swashplate. Thus, it is erroneous to equate balance output to hub loads without compensating for the pitch link loads in some manner.

A number of wind-tunnel test teams have attempted to use a dynamic calibration to overcome these issues (refs. 1–3). Using a shaker attached to the hub, these teams applied dynamic loads in different directions to compute the frequency response of the balance output relative to the applied hub loads. Using this data, they then determined dynamic amplification factors for the balance at the rotor harmonic frequencies. In some cases this work did not present the phase relationship between the applied hub loads and the balance output, and did not consider the coupling between the balance output channels. In addition, there is little discussion in the literature regarding the extent to which the predictions from comprehensive analysis were improved by the dynamic calibration.

Thus, the objective of the current work is to demonstrate the improvement that is achievable through the use of careful dynamic measurements of the testbed combined with incorporation of the testbed dynamics in the comprehensive analysis model of the system. This paper describes the dynamic testing of the Aeroelastic Rotor Experimental System (ARES), the model-scale conventional rotor system testbed in use at the Langley Transonic Dynamics Tunnel, including measurements of the balance frequency response and the modal response of the hub. In addition, the development of a detailed finite-element model of the ARES is described, along with its use in understanding the testbed dynamics. Finally, examples of the comparison between predicted and measured hub loads during wind-tunnel flight are presented and discussed.

OVERVIEW ON UTILIZING DYNAMIC MEASUREMENTS

Prior to presenting the results from the vibration testing of the ARES testbed, some discussion is needed to clarify what measurements are obtained from testing and exactly how these measurements can be utilized. The goal of this work is to develop a transformation so that analytically predicted dynamic hub loads can be transformed into predicted balance outputs

for comparison with experiment. In its simplest sense, this transformation is a six-by-six matrix that relates the hub forces and moments to the balance outputs. The static balance calibration is an example of this type of transformation, but it is not valid for dynamic loads. To develop a transformation for dynamic loads, the assumption is made that there exists a unique transformation matrix for each excitation frequency, and that system linearity permits the dynamic balance output to be identified by transforming the hub loads at each harmonic frequency. This transformation is commonly referred to as a "dynamic calibration." Unlike with a static calibration that only corrects amplitude, transformation matrices used in a dynamic calibration must be complex valued to account for phase changes that occur across the frequency spectrum. To develop this transformation, the balance output is measured during a series of vibration tests using a shaker to excite the ARES at the hub, and this output is used as the basis for the creation of an empirical transformation.

It should be emphasized that the measurements used to create the balance transformation are for the ARES testbed without most of the hub mass. Thus, the natural frequencies of the system will be different from those for the ARES including the hub and rotor system. Historically, researchers have included the hub during vibration testing, but this is not necessary, provided that the mass is accounted for in the comprehensive analysis. Applying excitation loads to the actual rotor hub can be challenging and can require additional fixtures that add mass to the system. In the present work, a "dummy" hub has been constructed, which replaces the rotor hub and provides attachment points for the shakers during testing. It is assumed that the difference in mass between the actual rotor hub and the dummy hub will be accounted for in the comprehensive model of the rotor system. Divorcing the rotor hub from the testbed during vibration testing also implies that the test results are a testbed property that can be utilized regardless of the rotor system attached to it. This is of particular interest to the authors, since there are multiple rotor hubs compatible with the ARES testbed.

Balance Transformation

The primary experimental test result that is being sought is a transformation relationship between the hub loads and the balance output as a function of frequency, but this is a synthesized result that must be created from the measured data. This transformation relationship is referred to herein as the balance transformation. First, a number of vibration tests are performed with a shaker connected at multiple points on the dummy hub and oriented in multiple directions. Each tests results in a measured frequency response function (FRF) for the six balance outputs relative to the applied load at the hub. Depending on the orientation and location of the excitation force, a combination of forces and moments are produced at the center of the hub. The nomenclature used for the balance outputs and the assumed coordinate system for the model is presented in Figure 1. The balance transformation for each FRF frequency is computed by solving for the 36 complex-value components of the matrix that satisfies the relationship

$$\begin{Bmatrix} N \\ A \\ P \\ R \\ Y \\ S \end{Bmatrix}_i = [T_{bal}] \begin{Bmatrix} F_x \\ F_y \\ F_z \\ M_x \\ M_y \\ M_z \end{Bmatrix}_i$$

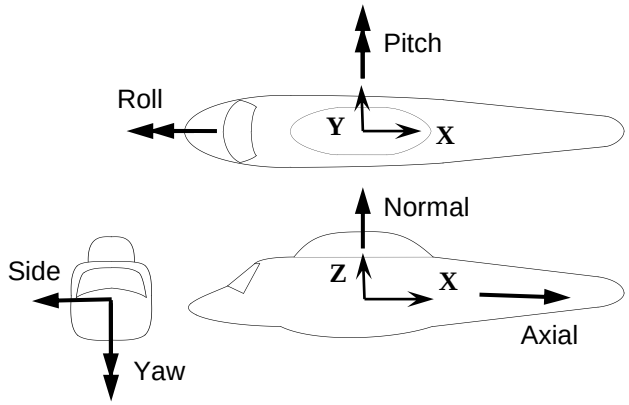

Figure 1. Model coordinate system and directions for positive balance outputs.

where *F* and *M* are the force and moment vectors at the hub, and *N*, *A*, *P*, *R*, *Y*, and *S* are the Normal force, Axial force, Pitch moment, Roll moment, Yaw moment, and Side force outputs of the balance for the i^{th} load case. This can also be expressed as

$$\boldsymbol{B}^i(\omega) = [T_{bal}](\omega) \cdot \boldsymbol{H}^i(\omega)$$

which emphasizes the fact that this transformation must be computed for each frequency (ω) in the FRF. If testing includes more than exactly six orthogonal excitation loads, then it is necessary to perform an averaging process to obtain a single balance transformation. This can be accomplished through the use of an H1 FRF estimator, just as was used to generate the FRF functions during the shake test. In this case, the cross-spectrum between the balance output and the applied loads is divided by the auto-spectrum of the applied loads. Thus, the matrix components of the balance transformation can be computed using

$$[T_{bal}]_{j,k}(\omega) = \frac{\sum_i \boldsymbol{B}_j^i(\omega) \cdot \boldsymbol{H}_k^i(\omega)^*}{\sum_i \boldsymbol{H}_k^i(\omega) \cdot \boldsymbol{H}_k^i(\omega)^*}$$

The balance transformation describes the balance output induced by the hub loads, but does not account for any loads transmitted via the pitch links. A similar process can be used to create a swashplate transformation to describe the relationship between the loads and moments induced by the pitch links and the balance output. Because these two separate load paths exist, inverting the balance transformation and using it to convert experimentally measured balance loads into hub loads is not necessarily valid. However, analysis-experiment comparison is most often done in this manner, and pitch link loads are combined with hub loads for comparison with transformed balance loads. This approach is only valid if the hub can be assumed to be rigidly connected to the swashplate such that they move together as a rigid body. A more mathematically reliable option would be to transform analytically predicted hub loads and pitch link loads into a predicted balance output that can then be compared to experimentally measured balance values, which is the approach taken herein.

Hub Modal Response

One issue that is typically ignored in rotor analysis, with the exception of stability analysis, is the effect of testbed motion and dynamics on the predicted hub loads. A testbed resonance that results in a large amplification between the hub loads and the balance output will also likely result in hub motion that may alter the loads transmitted from the rotor to the hub. Thus, the second test result of interest is the modal response of the ARES testbed. In particular, if acceleration measurements are made on the hub during the shake tests discussed above, it is possible to identify the modal response of the hub, which describes the motion of the hub induced by the applied hub loads. This modal response captures the dynamics of the testbed for the frequency range of interest and permits them to be incorporated into the comprehensive analysis of the rotor system.

The computation of the hub modes begins with measurement of hub acceleration FRFs during each vibration test. Since direct rotational measurements are not practical, measurements from tri-axial accelerometers are combined to derive the displacement and rotation of the point defined to be center of the hub in the comprehensive analysis. If more than exactly six orthogonal accelerations are measured during testing, then it is necessary to average them at each FRF frequency to obtain the six translational and rotational components of the hub motion. This averaging assumes that the dummy hub is rigid, which was shown to be approximately true for the ARES testbed in the frequency range of interest. The resulting six FRFs for each vibration test describe the six components of the hub acceleration as a function of the applied load for each test. There are numerous ways to extract modes from these FRFs, but it was decided that the most direct method was to use a technique identical to the balance transformation to create average FRFs and then extract modes from these. Reciprocity was enforced during creation of this hub transformation, so the components represent the idealized average FRFs of the hub motion for the six components of the hub load. A commercial software package was used to extract modes from these FRFs using a Rational Fraction Polynomial-Z method.

VIBRATION TESTING AND RESULTS

Demonstration of the techniques discussed above was performed on the ARES testbed with the goal of developing balance transformations and modal data that could be incorporated into a comprehensive model and used to create comparisons with wind-tunnel test results.

Setup

The ARES testbed, shown in Figure 2, is designed to support testing in the Langley Transonic Dynamics Tunnel of aeroelastically-scaled model rotor systems of up to approximately 10-ft diameter. Rotor systems on the ARES are powered by a variable-frequency synchronous motor rated at 47-hp output at 12,000 rpm. The motor is connected to the rotor shaft through a two-stage, belt-driven, speed reduction system. Rotor control is achieved using a conventional, hydraulically actuated rise-

and-fall swashplate system using three independent actuators. The testbed also has a hydraulically actuated pitch degree-of-freedom to achieve the rotor shaft tilt necessary for rotor system trim in forward flight. The shaft tilt range on the ARES is typically +8° (shaft back) to -18° (shaft forward). All rotor system drive and flight controls are shielded by generic fuselage skin panels. Custom hub configurations may be mounted on the ARES, however, the primary hub available currently is an articulated hub with coincident flap and lag hinges placed at the 3.0 inch radial station. Rotor systems tested on the ARES typically have a 1/rev rotating speed of 10.5 to 11.5 Hz, which provides Mach-scaling in the heavy-gas test medium of the TDT. During the current vibration testing, the hydraulic system was at standard operating pressure and the model was maintained at 0° shaft tilt. Vibration testing was conducted at other shaft tilts to examine the influence of shaft angle on the modal response.

Figure 2. The Aeroelastic Rotor Experimental System (ARES) model-scale helicopter rotor research testbed shown mounted in the test section of the Langley Transonic Dynamics Tunnel (TDT).

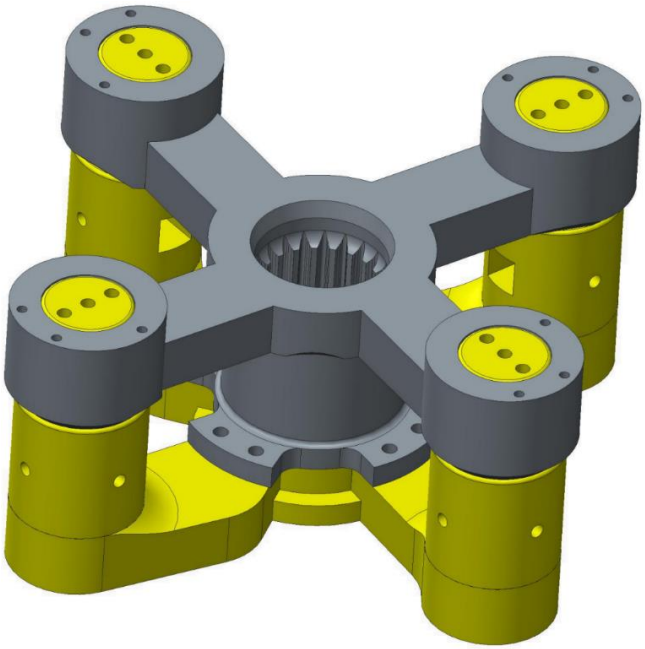

Figure 3. The "dummy" hub used during vibration testing of the ARES testbed to provide connectivity for shakers and accelerometers.

As discussed above, a "dummy" four-bladed hub was fabricated to permit application of shaker loads to the ARES testbed, as illustrated in Figure 3. The dummy hub has shaker and accelerometer mounting locations at points corresponding to the center of each hinge on the ARES articulated hub. Nonrotating radial, vertical, and lateral shaker loads were applied at each location, thereby inducing hub forces and moments in a manner similar to the actual rotor. The shaker was mounted to a reaction mass and suspended above the testbed. A variety of excitation modes were investigated, but the majority of measurements used a burst-random excitation with 0-200Hz frequency content and an 80-percent duration over an 8-second frame. Peak excitation was typically about ±10 lbf, although loads from 2 lbf to 15 lbf were tested to investigate system nonlinearity. Although ±10 lbf was smaller than harmonic loads often observed during wind-tunnel testing, system resonances resulted in peak balance outputs in the mid to upper portion of their ranges.

In addition to the six balance outputs and the four tri-axial accelerometers on the dummy hub, a number of other accelerometers were mounted on both the metric and nonmetric side of the ARES to permit quantification of the ARES mode shapes. These additional measurements were critical to identifying the modes for comparison with the developed finite-element model. Measured FRFs were computed from the average of forty frames to minimize noise, and were measured from 0-400Hz with a 0.125Hz interval.

Balance Output

Shaker loads were sequentially applied at all four rotor hinge positions along the three principal axes of the ARES. Since the shaker forces were applied at the hinge positions, each excitation typically induced both a force and moment about the hub center, except when the force was in the radial direction. The balance output from the resulting twelve sets of FRFs was used to form the balance transformation using the process presented above, which is not adversely affected by the fact that each set did not possess a pure hub force or moment. A sample of balance transformations is presented in Figures 4–6.

The response of the Normal and Axial balance outputs for hub excitation in the Z direction (vertical) is presented in Figure 4. These responses are what one would typically expect for a testbed. The magnitude of the Normal response is relatively flat and close to unity, with the exception of two peaks and a valley created by modes at 21 Hz and 41 Hz. The peak amplification value is 2.4, at the 21 Hz mode. The phase angle between the excitation and output is also close to zero, except in the vicinity of those two modes. The Axial balance output is largely unresponsive to the vertical excitation, except near the 41 Hz mode. One could almost make the case, based on these results, that the dynamic transformation is unnecessary, were it not for the fact that the mode at 41 Hz is close to the typical ARES 4/rev frequencies of 42–46 Hz.

The response of the Normal and Axial balance outputs for hub excitation in the X direction (axial), presented in Figure 5, tells a very different story. It is immediately clear that the response is highly dependent on the excitation frequency and that use of the static calibration values would result in loads being incorrect by as much as one order of magnitude. The Axial balance output has a magnitude that varies from 0.04 to 7.3 times the axial excitation load, and exhibits a phase angle that is approximately 180° for much of the frequency range. The dynamic response of the model also results in much greater coupling between the balance outputs, depending on the modes being excited at a given excitation frequency. For example, Normal output produced by the axial force at the hub is actually greater than the Axial output between 37 and 68 Hz. The complex nature of these results was more typical across the other balance outputs than the relatively simple response presented in Figure 4.

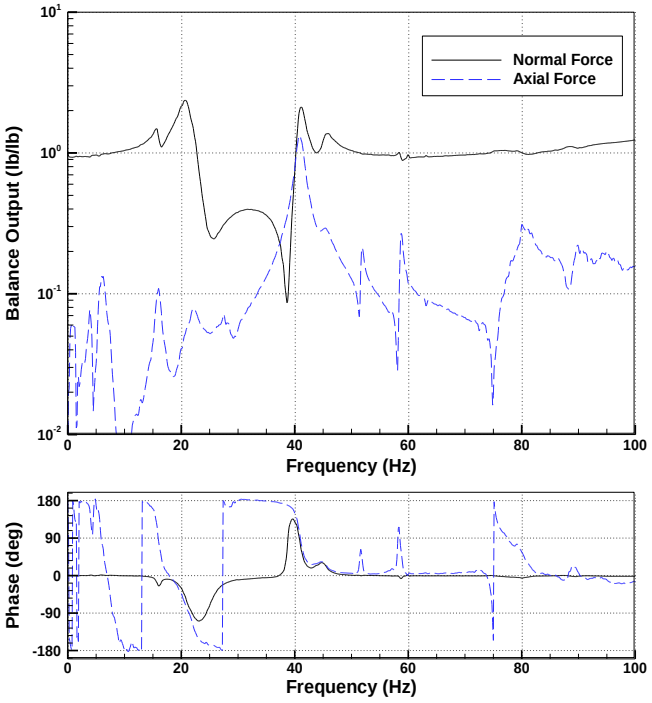

Figure 4. Balance transformation: Normal and Axial balance outputs to a hub force in the Z direction (Normal).

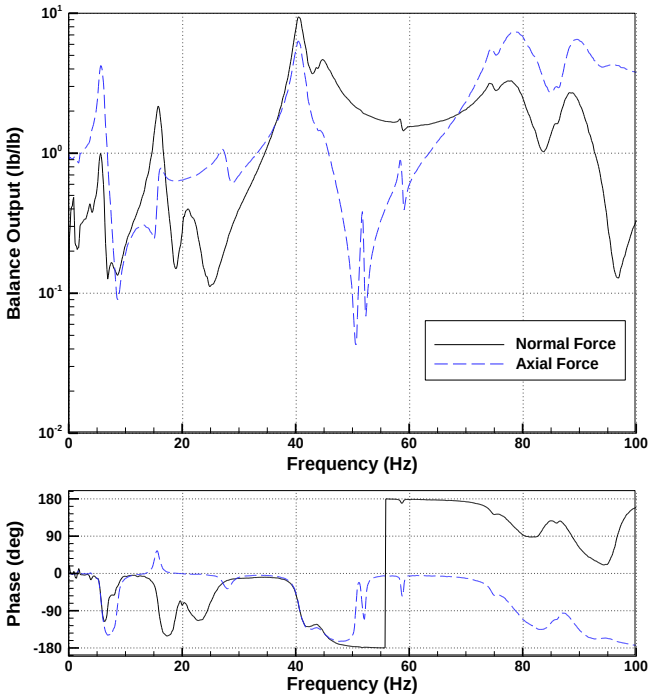

Figure 5. Balance transformation: Normal and Axial balance outputs to a hub force in the X direction (Axial).

Figure 6 presents the Pitch balance output for excitation in both the X and Z directions. Since the center of the balance is 1.75ft below the center of the hub, in-plane force at the hub results in significant Pitch and Roll outputs. The amplification of the Pitch output from an axial force varies between 0.03 and 11, relative to the static value. It is also interesting to note that above 41 Hz, the phase of the Pitch output switches. Ideally, a vertical force should not excite and Pitch output, but on the ARES the normal force induces significant Pitch output between approximately 20 and 50 Hz.

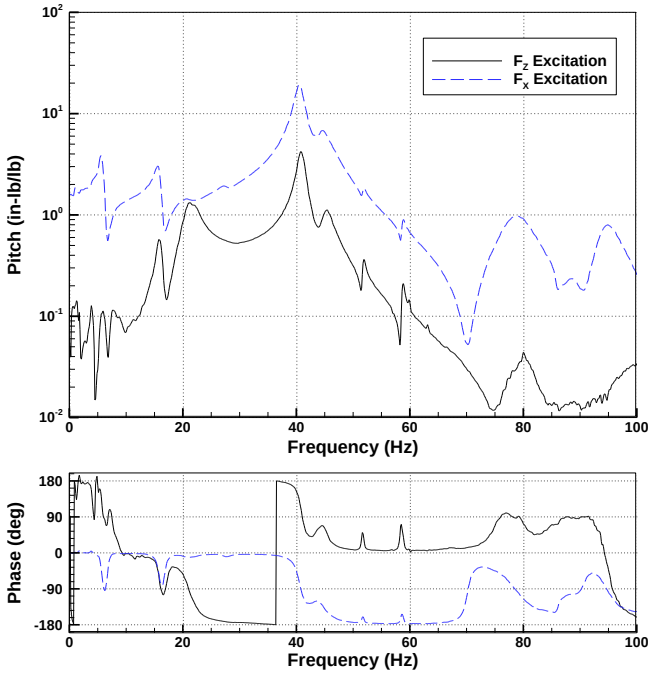

Figure 6. Balance transformation: Pitch balance output for hub forces in the X and Z directions (Axial and Normal).

Modal Response

The objectives of the modal test data acquired during hub excitation were to create a modal representation of the translational and rotational response of the hub, and to acquire sufficient accelerometer measurements over the ARES to be able to characterize the global nature of the measured modes. Using the data from four tri-axial accelerometers located on the dummy hub, the modal hub response was computed as described above. The first twenty primary hub modes are listed in Table 1. There were a number of other local modes that did not exhibit significant response at the hub, and were subsequently ignored. Note that the names listed for each mode are approximate descriptions for the overall character of the testbed deformation, and do not refer to any classical mode-shape definitions.

A comparison of the measured hub modes and the balance outputs presented in Figures 4–6 illustrates that not all modes contribute equally to the balance transformation. Although deformation at the balance flexure is a significant contributor to the modal response, it is not the only significant source of flexibility in the ARES. Thus, although the modes can generally be observed in the peaks of the balance transformation, there is minimal correlation between the transformation amplitudes and the magnitudes of the modal components. The magnitude of the peaks in the balance transformation are influenced not only by the amount of strain occurring in the balance flexures for a particular mode, but also by the degree to which that mode is excited by the dynamic load at the hub.

Table 1. Measured modal response at the hub (normalized by modal mass).

Mode	Frequency (Hz)	Damping (%)	Modal Mass (slug)	X (ft)	Y (ft)	Z (ft)	RX (rad)	RY (rad)	RZ (rad)
1	5.787	3.26	0.06852	-7.54E-2	-1.05E-2	1.27E-3	-1.03E-3	1.65E-2	-1.34E-3
2	5.805	5.06	0.06852	8.90E-3	8.60E-2	8.33E-4	1.26E-2	-7.50E-3	-2.86E-3
3	15.92	2.87	0.06852	-4.21E-2	-4.21E-3	-8.92E-3	2.22E-4	4.59E-2	-1.04E-3
4	21.26	5.92	0.06852	-1.16E-2	8.00E-4	-5.11E-2	3.72E-4	4.99E-3	5.09E-4
5	25.54	2.79	0.06852	0.0	-4.80E-2	0.0	-2.91E-2	3.29E-3	1.24E-2
6	40.70	1.68	0.06852	-1.05E-1	-6.72E-4	1.89E-2	3.04E-3	9.73E-2	-7.83E-4
7	44.85	3.92	0.06852	-7.36E-2	-3.91E-2	1.02E-2	-6.45E-3	6.58E-2	-6.01E-3
8	48.85	1.43	0.06852	1.50E-4	-3.11E-2	3.70E-4	-3.58E-2	1.61E-3	-3.39E-2
9	56.05	2.44	0.06852	7.17E-3	2.44E-1	-1.11E-3	1.92E-1	-2.15E-2	-4.69E-3
10	57.57	1.81	0.06852	5.28E-4	-7.25E-3	-8.24E-4	-1.83E-1	1.94E-2	1.38E-2
11	74.87	3.96	0.06852	-1.52E-1	-8.10E-3	-7.03E-3	-1.24E-3	1.13E-1	-2.22E-2
12	77.17	4.30	0.06852	-1.01E-1	-2.07E-2	-7.69E-4	7.54E-3	1.34E-1	-3.77E-3
13	79.06	2.13	0.06852	-5.22E-2	-4.61E-2	7.52E-4	-5.20E-2	4.15E-2	3.20E-2
14	88.41	1.68	0.06852	-9.17E-2	-1.45E-2	-2.64E-3	7.02E-3	1.05E-1	-3.40E-3
15	91.21	5.71	0.06852	1.86E-2	-6.70E-2	-5.50E-3	-1.09E-1	-1.40E-2	2.26E-2
16	107.6	1.53	0.06852	-1.23E-1	-4.12E-2	-1.20E-2	-5.39E-2	4.60E-2	-9.20E-2
17	107.8	2.34	0.06852	-4.28E-2	-1.20E-1	2.42E-3	-1.90E-1	4.64E-2	2.31E-2
18	119.1	3.68	0.06852	1.16E-1	2.85E-1	-8.77E-3	4.22E-1	-2.01E-1	-2.15E-2
19	128.3	4.00	0.06852	2.27E-1	-3.02E-2	-6.00E-2	-5.35E-2	-5.99E-1	1.92E-3
20	158.0	1.59	0.06852	2.20E-2	1.25E-3	7.73E-2	-1.20E-2	-5.18E-2	-2.51E-3

Test Variations

Additional testing was conducted to investigate if any of the natural frequencies changed due to physical state changes in the model. The first set of tests investigated variation in angle of attack, and the second set of tests investigated variation in hydraulic pressure. For the angle-of-attack variation, the shaker was set to act in the direction of the rotor so that the shaker is always normal or in-plane to the hub. Figure 7 and 8 presents the pitch and normal output due to an axial load at angles of attack 0°, -5°, and -10°. The frequency that is most significantly impacted is the 15 Hz mode, with an increase of 2 Hz from the 0° angle-of-attack to -10°. This mode was determined to be dominated by the pitch actuator. Intuitively, this makes sense because the length of the pitch actuator changes with angle of attack, and the inertia of the model has a slight rotation. To accurately model the effect due to the pitch actuator would be incredibly difficult and is beyond the scope of this work. In the current FEM model, the pitch actuator is connected between the post and model with a linear spring.

The pitch actuator is a hydraulically controlled actuator and is one significant unknown in the system for FEM modeling. This test varied the hydraulic pressure from 800 psi to 1800 psi with normal operating pressure between 1200 and 1500 psi. Figure 9 and 10 present the pitch and axial output for the variation in hydraulic pressure. From the figures, the shift in the 15 Hz mode is around 0.5 Hz, indicating that hydraulic pressure has some influence on system response. However, its effect is small compared to the effect of changes in the angle of attack.

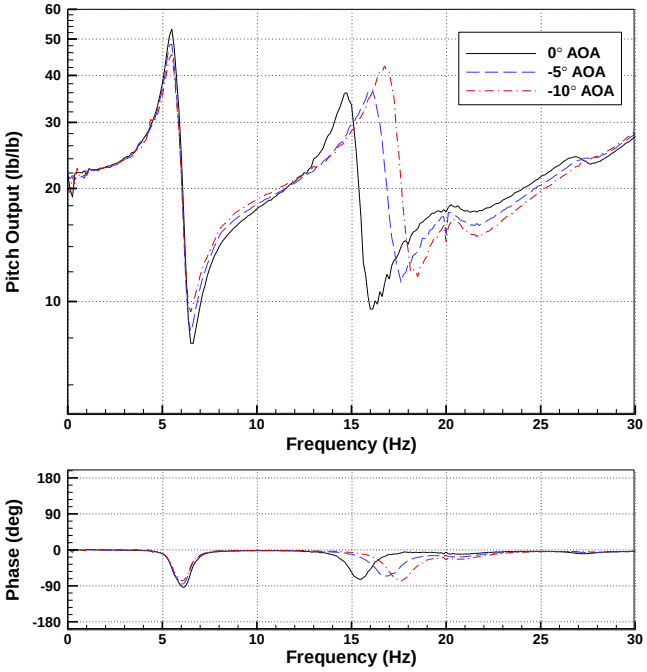

Figure 7. Balance transformation: Pitch balance output for hub forces in the X direction (Axial).

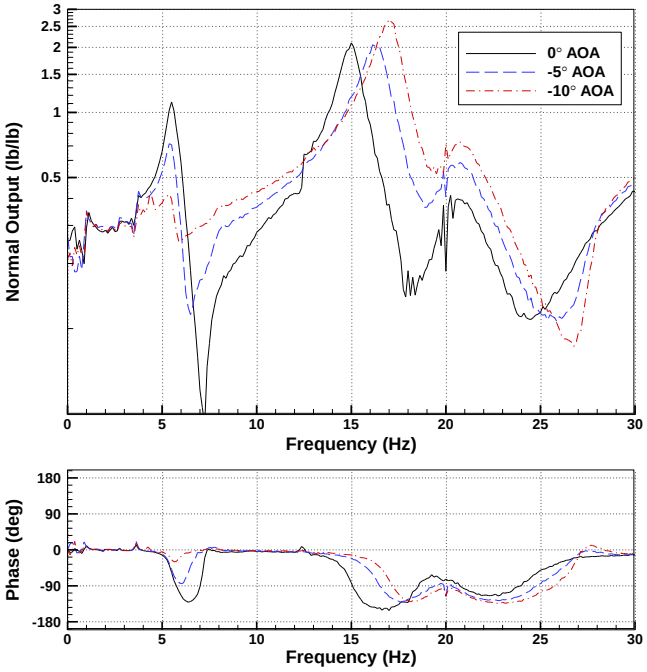

Figure 8. Balance transformation: Normal balance output for hub forces in the X direction (Axial).

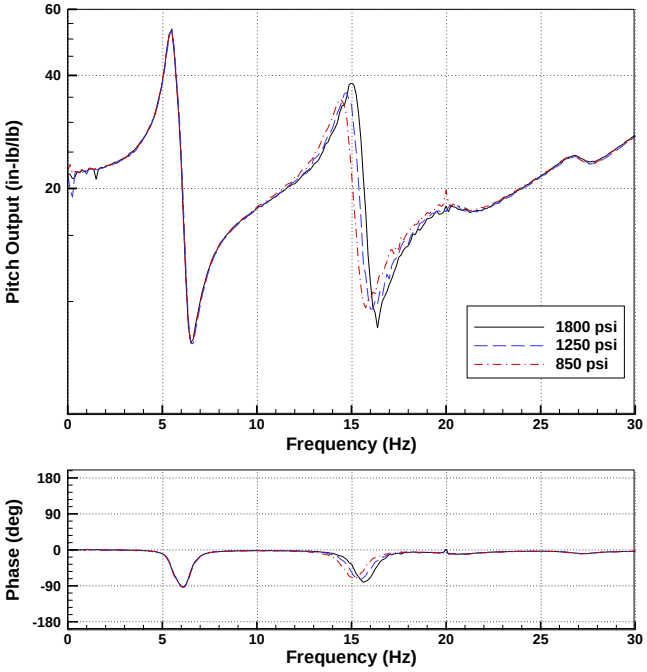

Figure 9. Balance transformation: Pitch balance output for hub forces in the X direction (Axial).

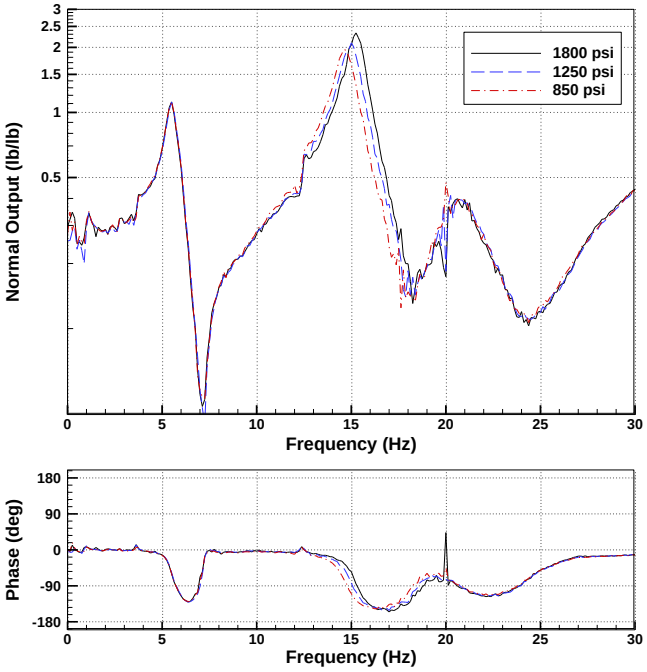

Figure 10. Balance transformation: Normal balance output for hub forces in the X direction (Axial).

FINITE-ELEMENT MODELING

In addition to performing a GVT to identify the dynamic response of the ARES, an ABAQUS finite-element model (FEM) was developed for use in predicting the modal behavior of the ARES. The objective for this model was to study ARES configuration changes to determine their effect on the rotor response. Also, if the model were of sufficient accuracy, it could be used to generate the modal hub motion for use in the comprehensive analysis, and possibly the balance transformation as well. In addition, the development of a finite-element model was used to provide insight into the sources of flexibility within the testbed and their effect on the dynamic response. The FEM was developed in stages using substructure models of individual components. This permitted verification of the model in stages using measured component masses and shake tests of sections of the ARES. In addition, this approach permits a library to be developed so that different model configurations can be studied. This section will describe how the model was developed, discuss results from the testing of each section, and present lessons learned during this process.

The development of the FEM began with modeling the lower portion of the stand, shown in Figure 11a. The ARES stand is mounted on foam-rubber pads to add flexibility and damping to prevent ground-resonance instabilities. The stiffness and damping of the foam rubber was unknown prior to experimental testing, but it was known that the stiffness was dependent on the torque applied to the mounting bolts during testbed installation. Modal testing demonstrated that the solid steel stand could be modeled very accurately using a combination of solid and shell elements. This provided a set of stiffness and damping values for the pads that were used in subsequent models. The resulting model predicted the first 14 natural frequencies to within 3 percent.

Next, the full stand was modeled, including all of the components below the pivot about which the ARES pitches (Figure 11b). This part of the ARES consists largely of solid sections with robust bolted joints (except for the foam-rubber pads). Consequently the FEM was able to accurately predict most of the first 16 natural frequencies to within 4 percent. The exception was the first two torsion modes. The first torsion mode is characterized by rigid-body rotation of the stand on the pads, and the second is characterized by elastic torsion of the stand coupled with rotation on the pads. The predicted natural frequencies for these modes were approximately 15 percent higher than observed. The source of this error seems to be that torsional response of the pads is nonlinearly dependent on the weight of the test stand. The response of the pads continued to vary slightly as other components were added to the ARES, and remained a source of error in all subsequent models.

A FEM of the balance was developed, with careful attention to accurately capturing the stiffness. The balance is a solid stainless steel component, which made solid modeling using CAD geometry relatively easy (Figure 11c). The thin flexures required a very fine mesh for the stiffness of the model to converge, and the final mesh had more than 3 million degrees of freedom. The predicted mass of the balance agreed with the measured mass to approximately 0.1 percent. The predicted natural frequencies were found to be highly dependent on the boundary conditions. Experimentally, frequencies were measured for the balance bolted to a heavy backstop, but predicted frequencies were found to vary depending on the area assumed to be in contact with the backstop. This result is similar to a conclusion found in prior work with bolted joints (ref. 4). Overall, the predicted frequencies agreed to within four percent. When one considers the uncertainty in material properties and the machining tolerances on the thin flexures, then these results are within the accuracy that is possible for this balance. One might consider replacing the detailed FEM with a simplified empirical representation of the balance, but based on the sensitivity to boundary conditions that was observed, this is something that would require great care to do accurately.

The components on the metric side of the balance were modeled as a single group and compared to modal testing of this section mounted to a heavy backstop rather than the balance. The metric side included the rotor-shaft housing, rotor shaft, dummy hub, swashplate, motor, drive sheaves, and belts. The FEM for this section is shown in Figure 11d, minus some components that are modeled as lumped masses, beams or springs, such as the swashplate, actuators and belts. The masses of individual components were computed and validated against measured values. Some components, such as the motor and bearings, required modeling using homogenized properties based on the measured mass. Drive belt stiffness was derived from the empirically measured drive system natural frequencies. This was necessary because the belt stiffness varied depending on the belt tension, which was controlled by turning locking nuts that adjust the length of threaded rods connecting the motor to an intermediate driveshaft housing and the intermediate driveshaft housing to the rotor-shaft housing. In addition to the threaded rods, there are also guide rods that travel through bronze bushings that keep the components aligned. This complex connectivity between the drive components was found to be very difficult to model using traditional finite-element methods. Estimating the bending stiffness of a threaded rod is always a tricky process, and the guide rods seemed to impose an intermediate constraint that was difficult to estimate empirically. As a result, predicted natural frequencies for the complete section were as much as 15 percent high for some modes and 15 percent low for others.

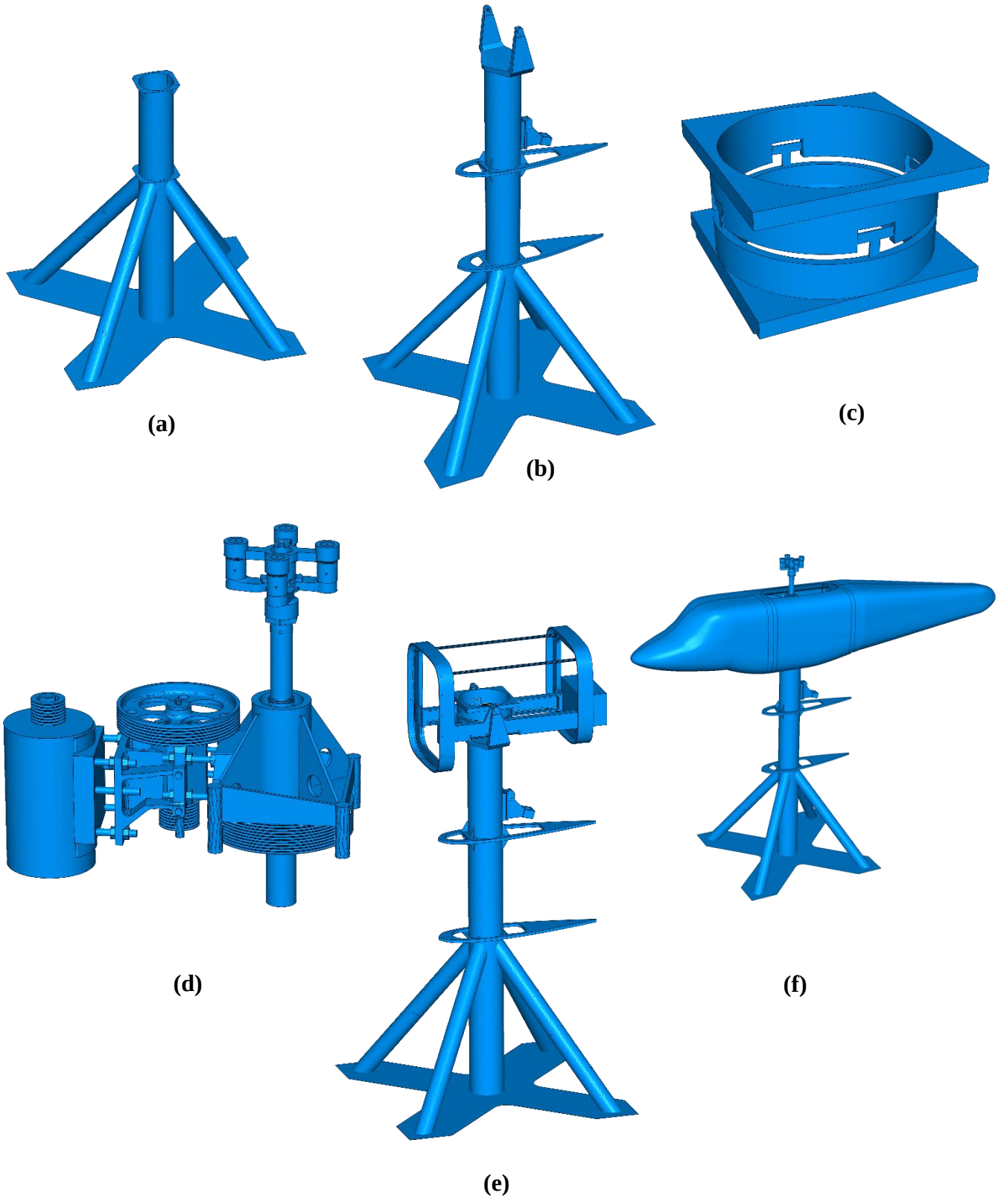

Figure 11. Finite-element models of the sections of the ARES investigated during vibration testing and development of the dynamic testbed model.

The fuselage was modeled using solid elements for the frame and shell elements for the skins. The FEMs of the skins were validated using mass measurements and measured free-free natural frequencies for each section. This fuselage model and the balance FEM were combined with the stand model and compared to modal testing of the ARES with nothing attached to the metric side of the balance (Figure 11e). The pitch pivot was modeled using a solid model of each pivot bolt connected to the stand and fuselage frame using distributed constraints. The pitch actuator was modeled using beams based on actuator geometry connected by a linear spring. One of the beams was assigned a coefficient of thermal expansion that permitted actuation to be simulated by prescribing a temperature change during analysis. Thus, the modal response of the ARES could be computed at various pitch angles through changes in actuator length. The linear spring stiffness was estimated by using the internal volume of the actuator and the bulk modulus of hydraulic oil (assumed to be 250 ksi). This was intended to be an initial guess before an empirical value could be derived, but modal testing revealed this to be a very reasonable approximation. The modal testing showed that the primary source of error was the modeling of the pitch pivot. The ideal model that was initially used was found to be too stiff, resulting in over-prediction of most of the natural frequencies. Addition of translation and rotation springs at the connection between the pivot bolt and the stand permitted some tuning of the model, but behavior seemed to be nonlinear and no single set of spring stiffnesses was able to capture the entire modal response accurately. The overall response of the FEM was reasonable and all observed modes were captured, but some natural frequencies were mis-predicted by as much as 20 percent, particularly yawing of the fuselage relative to the stand.

The issues with modeling the pivot connection and the connectivity of the metric-side components resulted in a final FEM that captures the general behavior of the ARES, but has significant errors in the predicted natural frequencies. The measured and predicted frequencies for the full model are presented in Table 2. The FEM predicts the number and sequence of the modes quite well, but there are differences in natural frequencies of almost 20 percent for some modes. Although these errors in the frequencies may not seem large, the location of these modes greatly affects the balance transformation. Because of the sharp peaks that can be observed in the balance transformations, a small shift in frequency may result in large changes in both the amplification and phase between the loads at the hub and output of the balance. Consequently, the resulting FEM is considered useful for studying the effect of configuration changes, but not of sufficient accuracy to replace vibration testing.

Table 2. Measured and predicted ARES natural frequencies.

Mode	Experimental (Hz)	FEM (Hz)	Mode
1	5.823	5.868	Rigid-body Axial
2	6.068	5.970	Rigid-body Side
3	12.44	14.17	Rigid-body Yaw
4	15.96	16.62	Model Pitch - actuator
5	21.22	19.34	Rigid-body Normal
6	25.39	20.38	Rigid-body Roll
7	27.60	24.01	Rigid-body Pitch
8	33.95	39.75	Fuselage-stand Yaw
9	40.77	45.61	Balance Pitch
10	44	52.79	Fairings
11	48.89	57.26	Fuselage Roll
12	56.05	53.86	Balance Side/Yaw
13	65.63	67.70	Balance Roll
14	74.73	84.00	Stand bending Axial
15	78.40	88.20	Stand bending Axial
16	88.51	85.58	Balance Normal
17	93.75	98.14	Fuselage Roll + skin
18	108.0	114.5	Fuselage Normal
19	118.1	124.2	Drivetrain
20	120.5	120.9	Fuselage Axial

COMPARISON BETWEEN ANALYSIS AND EXPERIMENT

Finally, a study was conducted to determine the impact of using the balance transformation on predicted balance harmonics in comparison with experimentally measured results obtained during a wind-tunnel test. The experimental data used for comparison were from wind-tunnel testing of a set of Active-Twist Rotor (ATR) blades, which had undergone extensive bench testing to validate the structural model used in the comprehensive analysis (ref. 5). This rotor system was tested in heavy gas in the Langley Transonic Dynamics Tunnel. Two forward-flight test cases, presented in Table 3, were chosen for comparison of the comprehensive analysis and the experimental measurements, one low-speed and the other high-speed. Although these blades are capable of actively twisting during flight, in both of these test cases, the blades were unactuated.

Table 3. Wind-tunnel test cases used for balance output comparison.

Mode	Low-Speed	High-Speed
Advance Ratio	0.127	0.335
Shaft Angle (deg)	-1.5	-9.5
Rotor Speed (RPM)	604	604
Coefficient of lift / solidity	0.0715	0.0715

The tested ATR has a radius of 63.36 in. and was operated at 604 RPM to achieve a tip Mach number of 0.63. The blades have a constant 4.64-in chord, a built-in -9deg/R linear twist, and the outer 0.07R span of the blades are swept aft by 20 deg. Further details regarding the design of the blades can be found in reference 5. The rotor blade beam properties were computed using UM/VABS, a finite element analysis that computes beam properties for arbitrary cross-sectional configurations (ref. 6). The beam properties were used within the comprehensive analysis CAMRAD II, and verified through a series of cantilevered and free-free vibration tests (ref. 5).

CAMRAD II is a rotorcraft aeromechanics analysis tool that combines a nonlinear finite element solution with multibody dynamics (ref. 7). A lifting line model is employed with varying complexities of wake models. To supplement the aerodynamic model within CAMRAD II (CSD analysis), the solution was coupled with a CFD solver, FUN3D. The CFD mesh includes 4.6 million nodes for the rotor and 2.1 million nodes for the overset mesh, which includes the rigid fuselage geometry (ref. 8). For hub load calculation, CAMRAD II uses a harmonic balance method. The predicted hub forces and moments were converted into predicted balance outputs using the empirical balance transformation developed above. The complex valued transformations at the first 10 harmonic frequencies were interpolated from the empirical balance transformation function, which had a 0.125Hz interval. The comparisons were made between the predicted and measured balance harmonics, and in addition, these were used to generate synthesized waveforms over the rotor azimuth.

Figure 12 presents hub loads for the low-speed forward flight results for CFD/CSD coupling in the time domain for one rotor revolution. The case was run using a single blade analysis with no fixed system modes. The red line shows the traditional method of predicting the balance output, by taking the predicted hub loads and applying only the moment arm induced by the height of the hub above the balance. The blue line shows the balance output after the dynamic calibration has been applied to the predicted hub loads, and the black line represents the experimental data. In general, the traditional balance output predictions are significantly smaller in magnitude than the measured values. Since the dynamic balance response is dominated by the 4/Rev harmonics, the large amplification created by the modes near this frequency results in a dramatic increase in the predicted balance outputs. However, the use of the balance transformation over-predicts the experimental loads by more than double in some cases. The only case which appears reasonably accurate is the Side force, which was only slightly increased by the balance transformation.

As discussed above, the large balance amplification likely implies that the testbed will exhibit sufficient motion to alter the rotor loads transmitted to the hub. Flexibility of the fixed frame can be modeled in CAMRAD II using mode shapes. Of the ARES hub modes identified in Table 1, the 16 dominant modes were used to simulate airframe flexibility through 8/Rev. For purposes of reduced complexity, the CFD/CSD coupling was trimmed and converged without fuselage modes, which resulted in significant computational savings. The modes were then introduced as a final CSD cycle using CFD airloads and multi-blade analysis. The hub loads, in particular their phase angles, were found to be very sensitive to the convergence tolerances used in the comprehensive analysis computational loops that control airframe response, rotor trim, and the motion coupling the airframe and the rotor.

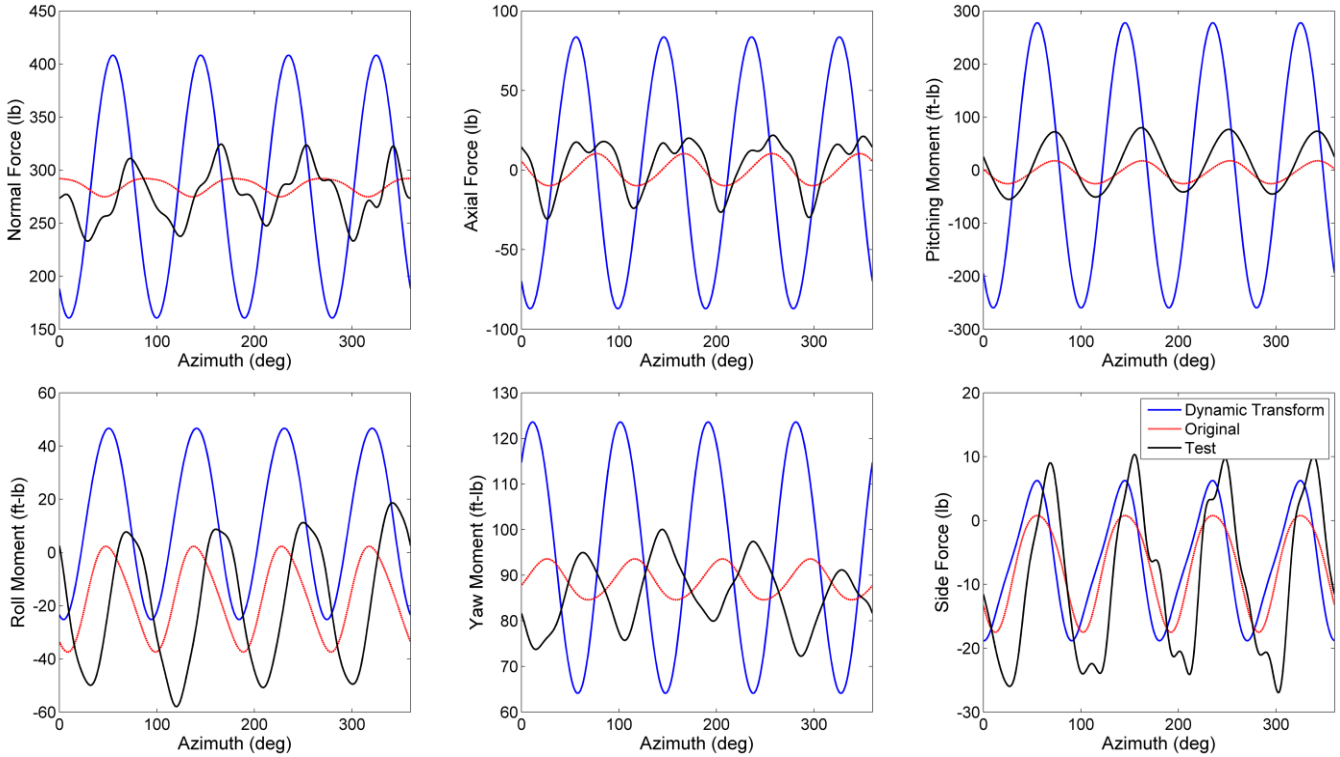

Figure 12. Balance output for the low-speed test case with CFD/CSD coupling, single blade analysis, and no fixed system modes.

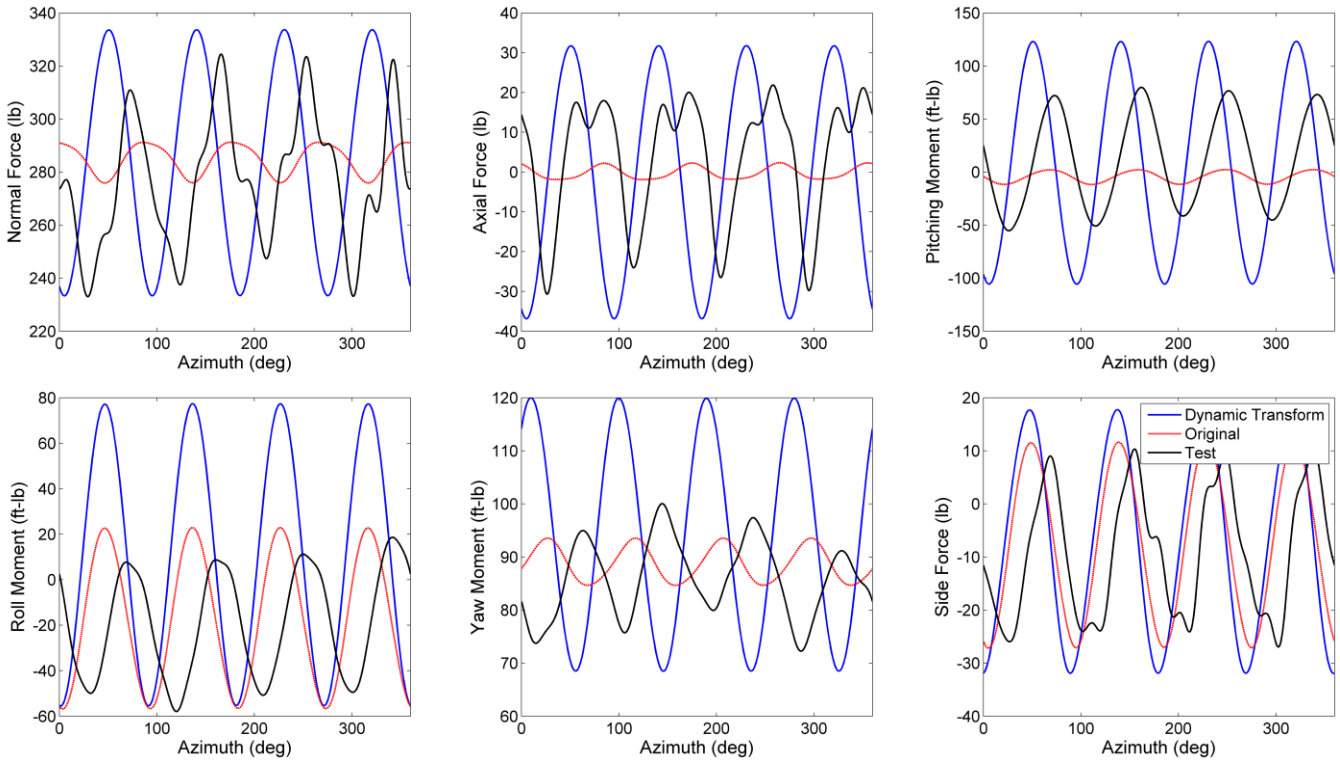

Figure 13. Balance output for the low-speed test case with CFD/CSD coupling, multi-blade analysis, and with fixed system modes.

The results for the low-speed case using multi-blade analysis coupled with fixed system modes, are presented in Figure 13. The most significant result from the use of the fuselage modes was the reduction in the Normal, Axial and Pitch outputs for the predictions using the balance transformation, which results in better correlation with the experimental data. The 4/Rev predicted load magnitudes for each output are reasonably close to the experimental levels observed during the test. However, there is relatively poor agreement for the Roll and Yaw outputs, and there are still differences in the phase between the predicted and measured outputs.

The effect that the balance transformation has on the 4/Rev balance outputs can be better understood by examining the contributions from each hub component, as detailed in Table 4. Each row represents the contribution of each component of the hub force and moment to a specific balance output, and the complex sum of these components is the net balance output at 4/Rev. The coupling between the axial force and the pitch moment at the hub and the Normal and Axial balance outputs is particularly noteworthy. Not only does the 2.04-lb 4/Rev axial force at the hub get amplified to a 12.3-lb Axial output, but it also contributes 17.9 lb to the Normal output. In addition, the 6.43-ft-lb 4/Rev pitching moment at the hub contributes 29.0 lb to the Axial output and 44.8 lb to the Normal output. Thus, the 4/Rev Normal output from the balance exhibits very little correlation to the 7.51-lb 4/Rev vertical force at the hub. Since the net balance output is a complex-valued sum, it is clear that accurate accounting of the phase angles in both the predicted hub loads and the balance transformation is required to accurately predict these balance outputs.

The results from the high-speed case are very similar to those from the low-speed case. The CFD/CSD coupled results presented in Figure 14 over-predict the response when the dynamic calibration is applied to the single blade analysis with no fixed system modes. When fuselage modes are introduced into the model, the predicted 4P balance load correlates reasonably well with the test data, as presented in Figure 15. The 8/Rev harmonic evident in the experimental Axial and Normal outputs was not captured by the comprehensive analysis for either the low-speed or high-speed case.

Table 4. Component-level breakdown of the 4/Rev predicted balance output for the low-speed test case.

	Analytical	F_x	F_y	F_z	M_x	M_y	M_z		
	4/Rev Hub Load	2.04 lb -23.2°	19.3 lb -18.0°	7.51 lb -1.9°	7.88 ft-lb 28.7°	6.43 ft-lb -58.1°	4.39 ft-lb 78.2°		
		Hub Load Contribution (Magnitude and Phase)						Net	Experiment
4/Rev Balance Output	Normal (lb)	17.9 -84.2°	3.4 23.0°	8.3 125.3°	0.5 125.3°	44.8 -167.4°	2.8 171.0°	50.1 -158.1°	31.5 -57.9°
	Axial (lb)	12.3 -82.6°	3.2 27.2°	7.4 143.0°	0.4 -145.4°	29.0 -167.7°	1.8 -168.7°	34.3 158.5°	19.3 -70.9°
	Pitch (ft-lb)	37.4 -81.2°	8.3 28.5°	24.6 147.4°	1.3 140.9°	94.4 -164.0°	5.4 175.4°	114.3 156.7°	61.5 -74.0°
	Roll (ft-lb)	0.7 -102.7°	55.2 -164.2°	0.3 121.6°	13.2 -149.6°	1.1 140.5°	1.1 109.4°	66.4 173.8°	32.2 -64.3°
	Yaw (ft-lb)	2.2 68.4°	13.4 12.3°	1.1 -58.8°	1.1 -18.2°	4.8 -5.0°	13.7 94.0°	25.7 -40.8°	9.2 -117.6°
	Side (lb)	0.5 -64.7°	22.9 -164.7°	0.2 160.5°	1.9 142.9°	0.6 -156.2°	4.5 95.0°	24.7 177.6°	16.2 -95.8°

Based on the results from the two comparison cases, the dynamic calibration method appears very promising, but there are a number of issues limiting the accuracy of the predicted balance outputs. The apparent sensitivity of the comprehensive analysis to convergence and trim tolerances, particularly with regard to the CFD/CSD coupling and the inclusion of fuselage modes, limits the authors' confidence in the repeatability of the results until a broader array of test cases can be assessed. Additional CFD coupling cycles may be required, since best practices have not yet been established for CFD/CSD coupling with fixed frame modes.

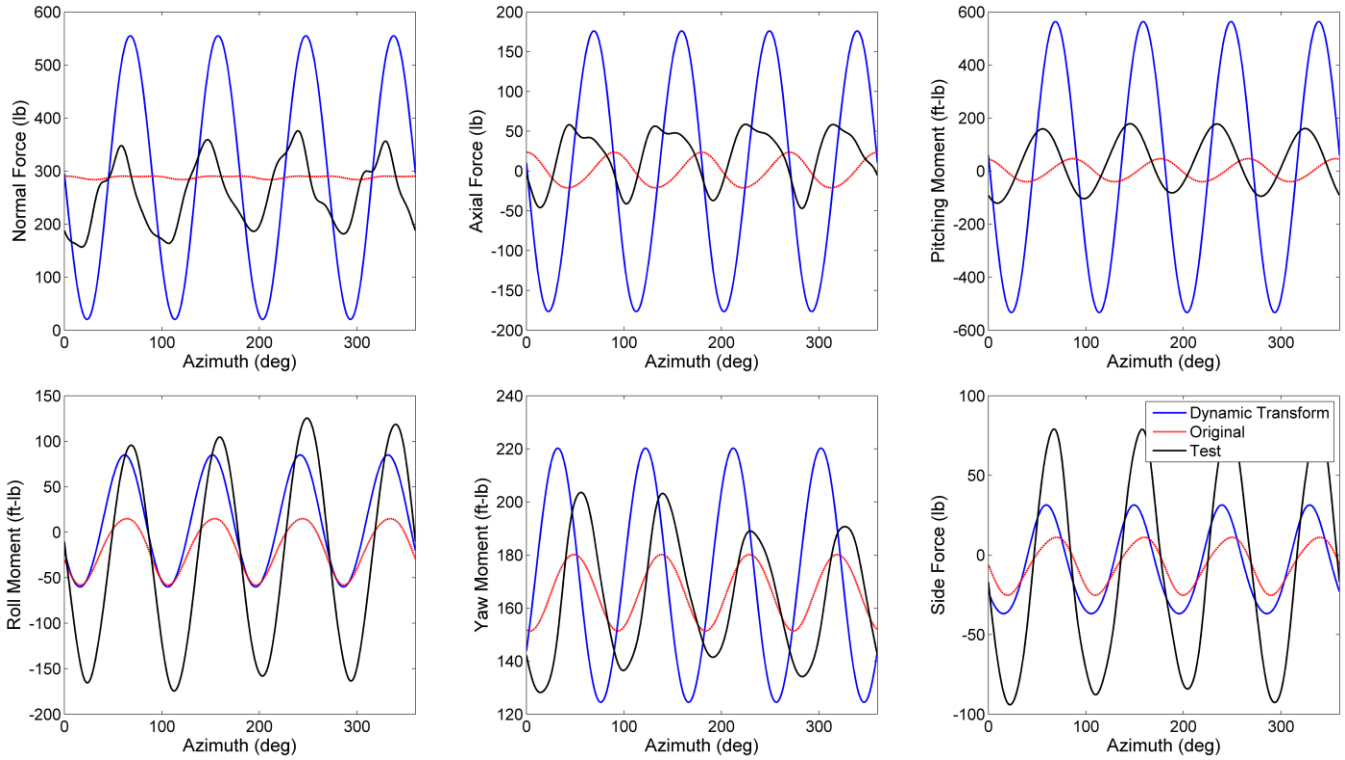

Figure 14. Balance output for the high-speed test case with CFD/CSD coupling, single blade analysis, and no fixed system modes.

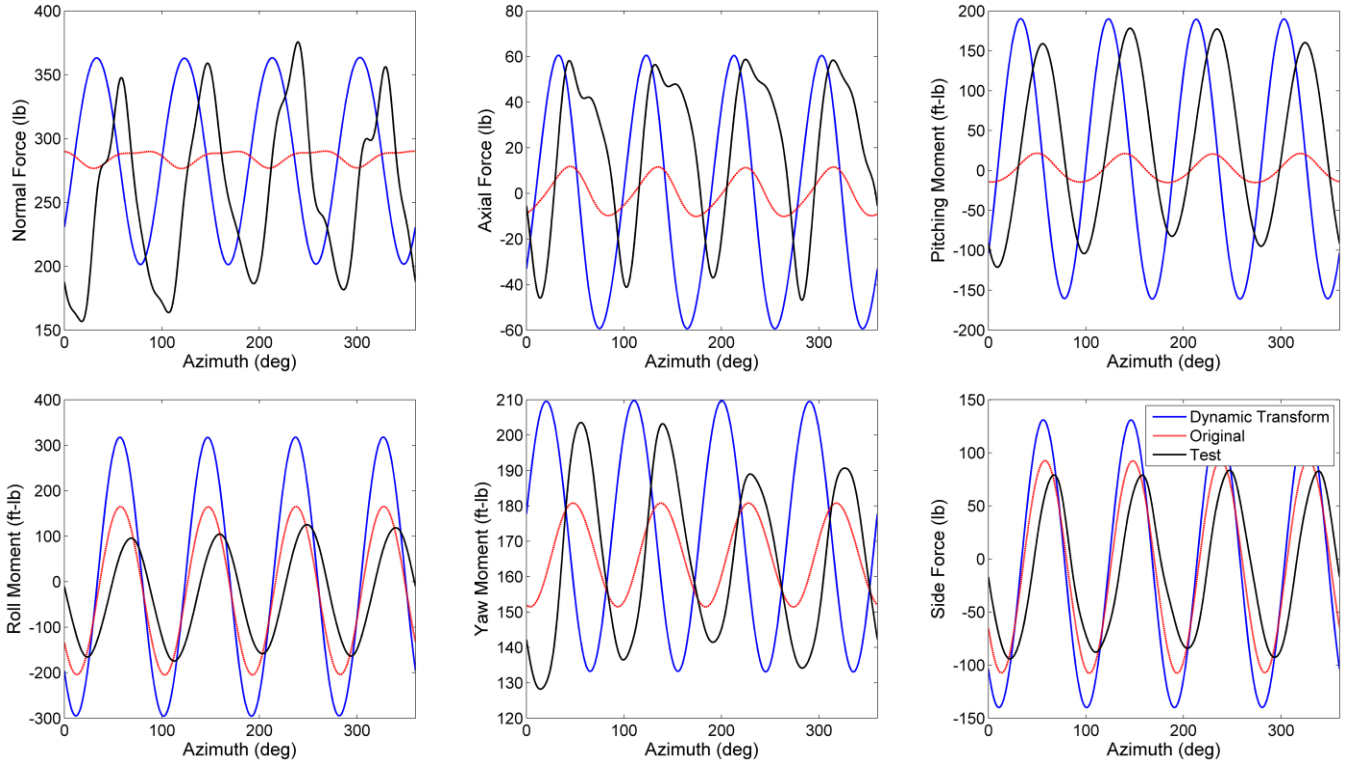

Figure 15. Balance output for the high-speed test case with CFD/CSD coupling, multi-blade analysis, and with fixed system modes.

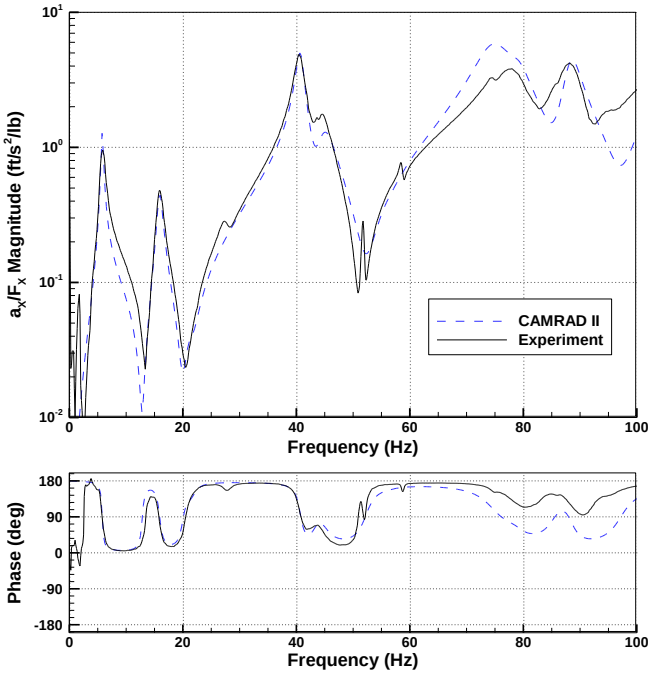

Figure 16. Measured and simulated hub acceleration in the axial direction induced by an axial force at the hub.

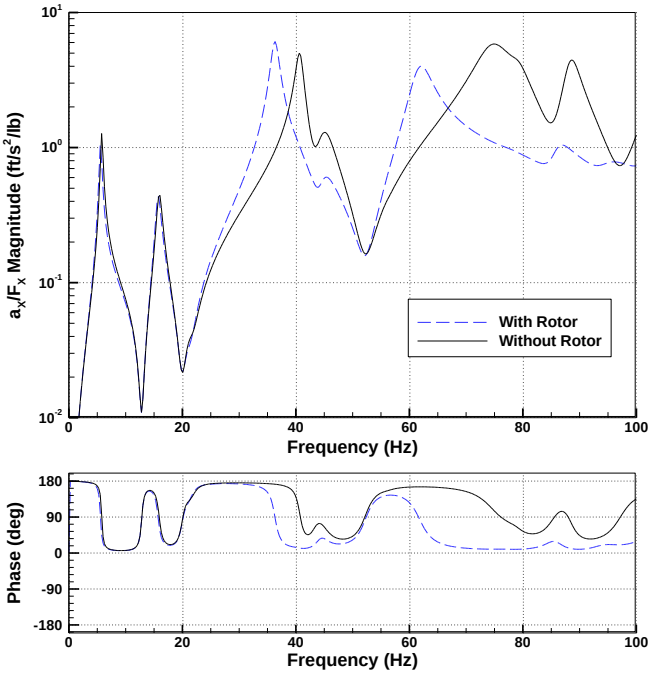

Figure 17. Effect of rotor mass on the simulated hub acceleration in the axial direction induced by an axial force at the hub.

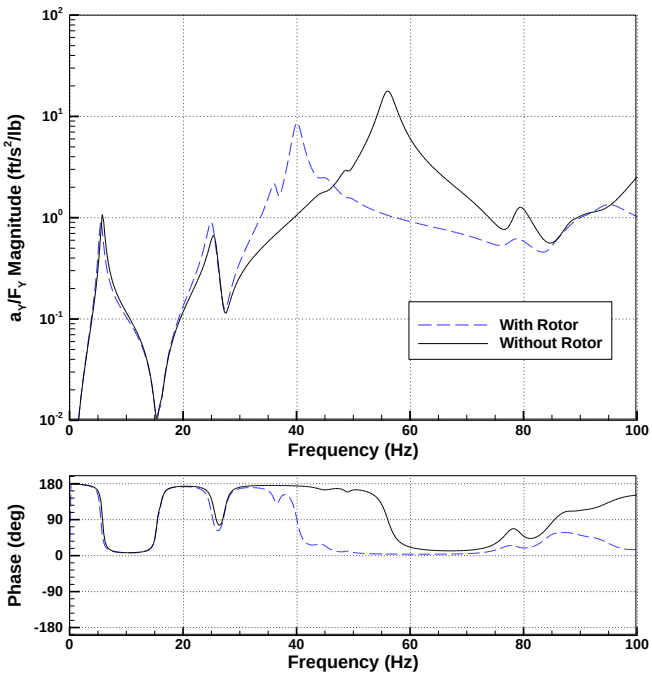

Figure 18. Effect of rotor mass on the simulated hub acceleration in the side direction induced by a side force at the hub.

Another source of error in the predicted balance output comes from the limitation of the modal approximation used to simulate testbed motion at the hub. First, the modes are derived from a synthesis of twelve separate shake tests, and the nonlinear aspects of the response are effectively averaged out. In addition, modes extracted from the average response are assumed to be linear, and smaller local modes are ignored. The net result of this is that the response simulated by the modal representation can only be described as an approximation of the actual testbed response. This can be observed in Figure 16, which presents the

frequency response of the hub acceleration in the axial direction due to an axial force at the hub. The experimental response from the shake tests is compared to the acceleration predicted by CAMRAD II using the synthesized modes. Not only does the experimental result show a number of small variations induced by local modes not included in the analysis, but at high frequencies the testbed begins to exhibit a response that is beyond what the modal approximation can simulate.

Also, the frequencies of modes in the vicinity of 4/Rev were observed to be highly influenced by the addition of mass above the balance. The effect of adding the rotor mass is shown in Figures 17 and 18, which present the frequency response of the hub acceleration in the axial direction due to an axial force at the hub and the acceleration in the side direction due to a side force, respectively. The addition of the rotor mass results in the axial mode at 41 Hz being reduced to 37 Hz, significantly altering its influence at 4/Rev. Also, the side mode at 56 Hz without the rotor shifts to almost exactly the 4/Rev frequency, indicating that this mode is extremely sensitive to changes in the mass. The testbed with a spinning rotor will, of course, exhibit different natural frequencies, but it is clear that this modal activity in the vicinity of the 4/Rev harmonic frequency greatly impacts the accuracy of any predicted loads.

CONCLUSIONS

This work presented results from an effort to develop a dynamic calibration of the Aeroelastic Rotor Experimental System (ARES) model-scale rotor system testbed. The mathematical development of the balance transformation was described, along with the experimental testing used as the basis for this transformation. In addition, a detailed finite-element model of the ARES was developed and compared to modal measurements for the testbed. Finally, examples of the comparison between predicted and measured hub loads during wind-tunnel flight were presented and discussed. Based on the work presented herein, the following conclusions were made.

- Based on the two wind-tunnel test cases examined, the use of the balance transformation has the ability to significantly improve the correlation between predicted and measured balance outputs.
- Incorporation of the fuselage modes into the comprehensive analysis appears to be necessary for effective use of the balance transformation.
- The ARES testbed exhibits several natural frequencies near the 4/Rev rotor frequency, resulting in a balance transformation that has large amplification and is very sensitive to model changes. This greatly limits the accuracy of the developed dynamic calibration.
- Although most of the components of the ARES could be accurately modeled using finite-elements, modeling the connectivity between the components was found to be significantly challenging. This resulted in the final FEM having insufficient accuracy to replace vibration testing, but still being useful for studying the effect of configuration changes.

Based on the behavior exhibited by the ARES testbed, future work will center on verification of the modal response and accuracy of the balance transformation at the 4/Rev frequency. The use of tuned-mass dampers and the addition of mass will be investigated to mitigate the testbed vibration mode near the 4/Rev frequency, which could help reduce the amplification of balance loads at this frequency. Also, since the modal response of the testbed near this frequency appears to be highly dependent on the mass attached to the metric side of the balance, sensitivity to swashplate position and blade mass requires further investigation to ensure the accuracy of the balance transformation.

ACKKNOWLEDGEMENTS

The authors would like to acknowledge the NASA Rotary Wing program and Steve Massey for the CFD support they provided.

Author contact: Andrew Kreshock Andrew.R.Kreshock.civ@mail.mil
Robert.P.Thornburgh.civ@mail.mil, , Matthew Wilbur Matthew.L.Wilbur.civ@mail.mil

REFERENCES

[1]Russell, C. R., "Shake Test Results and Dynamic Calibration Efforts for the Large Rotor Test Apparatus," Fifth Decennial Specialists' Meeting on Aeromechanics, San Francisco, California, January 22-23, 2014.

[2]Nguyen, K., and Lau, B., "Dynamics of the McDonnell Douglas Large Scale Dynamic Rig and Dynamic Calibration of

the Rotor Balance," NASA TM 108855, October 1994.

[3]Peterson, R. L., and van Aken, J. M., "Dynamic Calibration of the NASA Ames Rotor Test Apparatus Steady/Dynamic Rotor Balance," NASA TM 110393, April 1996.

[4]Thornburgh, R. P., Floersheim, R. B., and Hou, G. J. -W., "An Analytical and Experimental Study of a Scaled Helicopter Tailcone," 49th AIAA/ASME/ASCE/AHS/ASC Structures, Structural Dynamics, and Materials Conference, Schaumburg, Illinois, April 7-10, 2008.

[5]Kreshock, A. R., Thornburgh, R. P., Wilbur, M. W., and Langston, C. W., "Experimental Bench Testing of an Active-Twist Rotor Blade," 53rd AIAA/ASME/ASCE/AHS/ASC Structures, Structural Dynamics, and Materials Conference, Honolulu, Hawaii, April 23-26, 2012.

[6]Palacios, R. and Cesnik, C., "Cross-Sectional Analysis of Nonhomogeneous Anisotropic Active Slender Structures," *AIAA Journal*, Vol. 43, No. 12, 2005, pp. 2624-2638.

[7]Johnson, W., *Comprehensive Analytical Model of Rotorcraft Aerodynamics and Dynamics II v4.6*, Palo Alto, CA, 2007.

[8]Massey, S. J., Kreshock, A. R., and Sekula, M. K., "Coupled CFD/CSD Analysis of Rotor Blade Structural Loads with Experimental Validation," Paper 2013–3158, 31st AIAA Applied Aerodynamics Conference Proceedings, June 2013.

APPENDIX A: COMPLETE BALANCE TRANSFORMATION

The balance transformation functions are developed from a number of vibration tests performed with a shaker connected at multiple points on the dummy hub and oriented in multiple directions. Each of these tests results in a measured frequency response function (FRF) for the six balance outputs relative to the applied load at the hub. Depending on the orientation and location of the excitation force, a combination of forces and moments are produced at the center of the hub. A sufficient independent load directions allows the transformation functions to be resolved from the FRFs. The following figures present the balance transformation function which includes 36 components to represent all direct interactions and coupling terms.

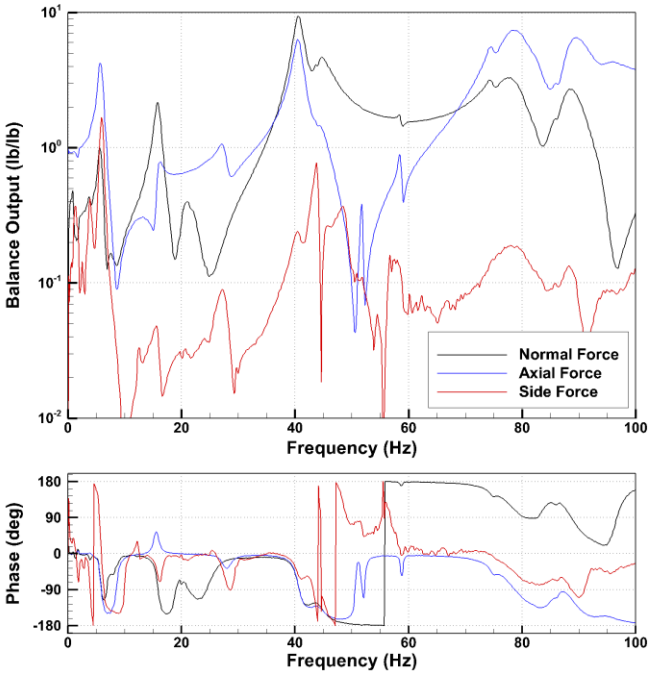

Figure A.1. Balance transformation: Normal, Axial, and Side balance outputs to a hub force in the X direction (Axial).

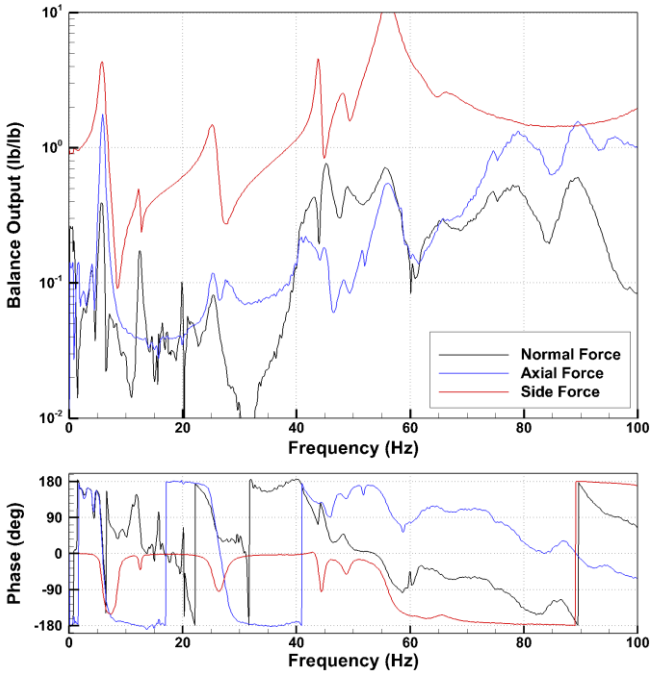

Figure A.2. Balance transformation: Normal, Axial, and Side balance outputs to a hub force in the Y direction (Side).

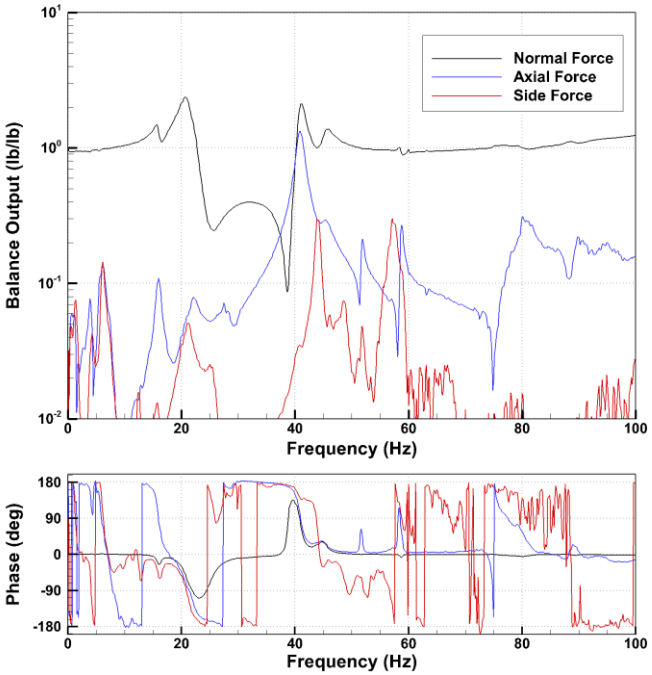

Figure A.3. Balance transformation: Normal, Axial, and Side balance outputs to a hub force in the Z direction (Normal).

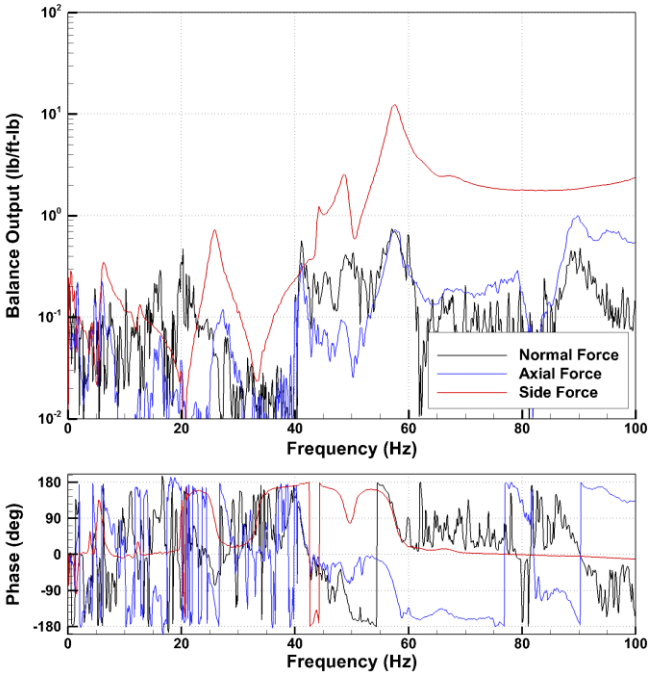

Figure A.4. Balance transformation: Normal, Axial, and Side balance outputs to a hub moment about the X direction (Roll).

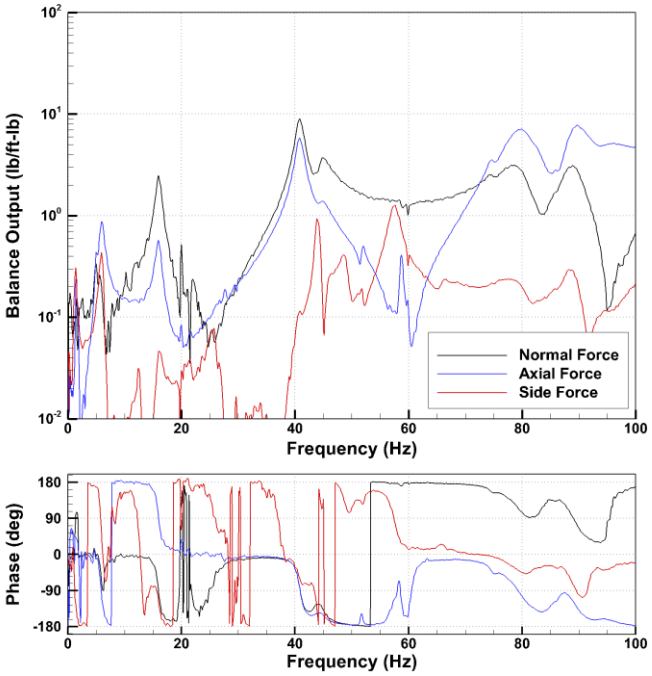

Figure A.5. Balance transformation: Normal, Axial, and Side balance outputs to a hub moment about the Y direction (Pitch).

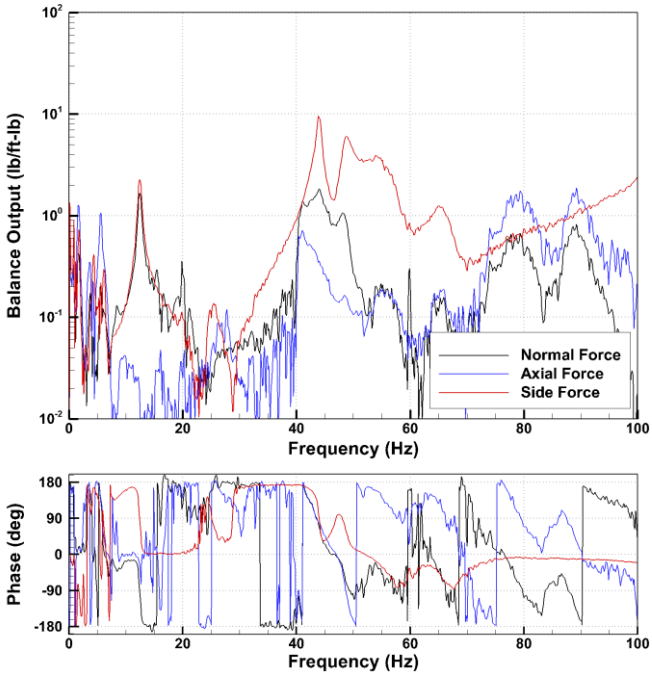

Figure A.6. Balance transformation: Normal, Axial, and Side balance outputs to a hub moment about the Z direction (Yaw).

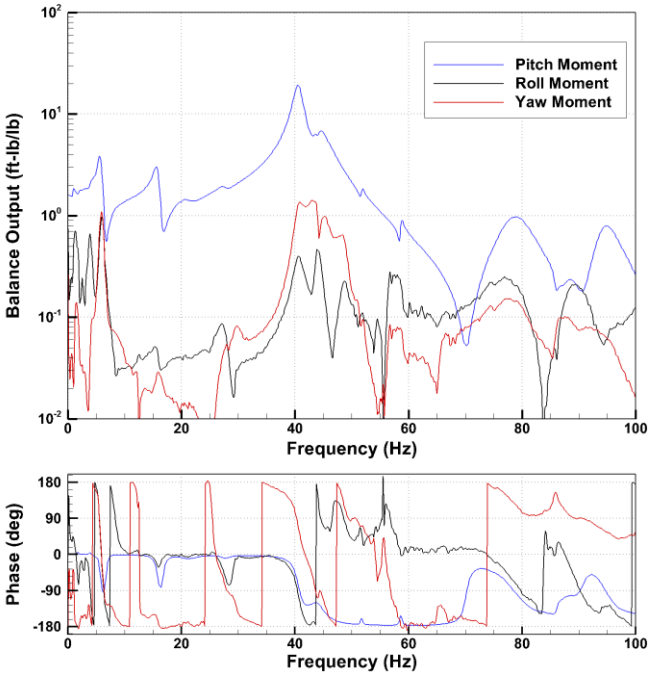

Figure A.7. Balance transformation: Pitch, Roll, and Yaw balance outputs to a hub force in the X direction (Axial).

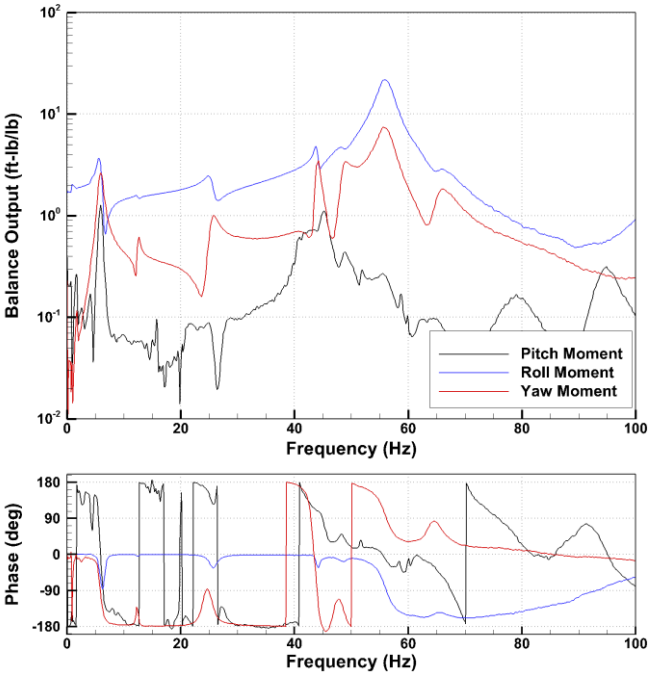

Figure A.8. Balance transformation: Pitch, Roll, and Yaw balance outputs to a hub force in the Y direction (Side).

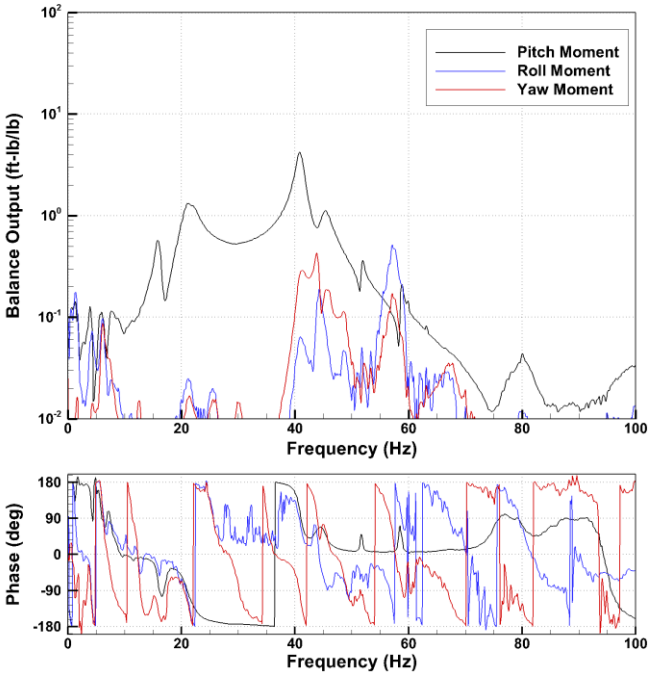

Figure A.9. Balance transformation: Pitch, Roll, and Yaw balance outputs to a hub force in the Z direction (Normal).

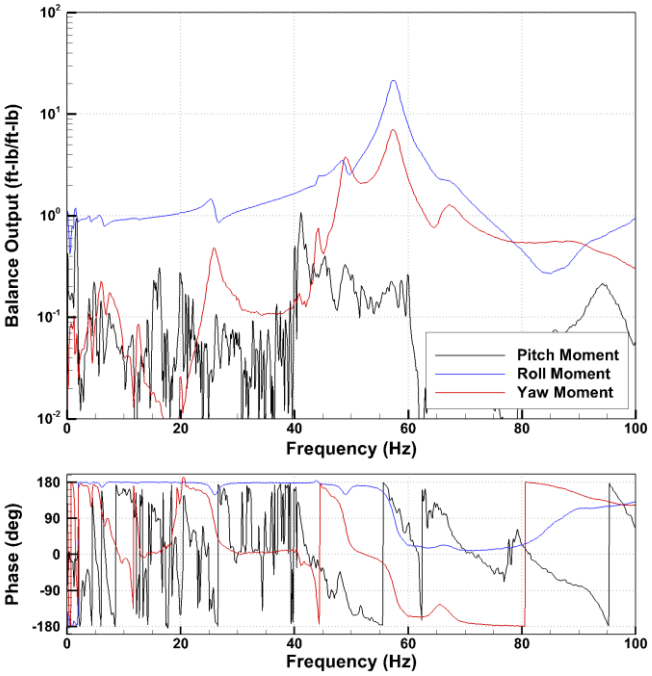

Figure A.10. Balance transformation: Pitch, Roll, and Yaw balance outputs to a hub moment in the X direction (Roll).

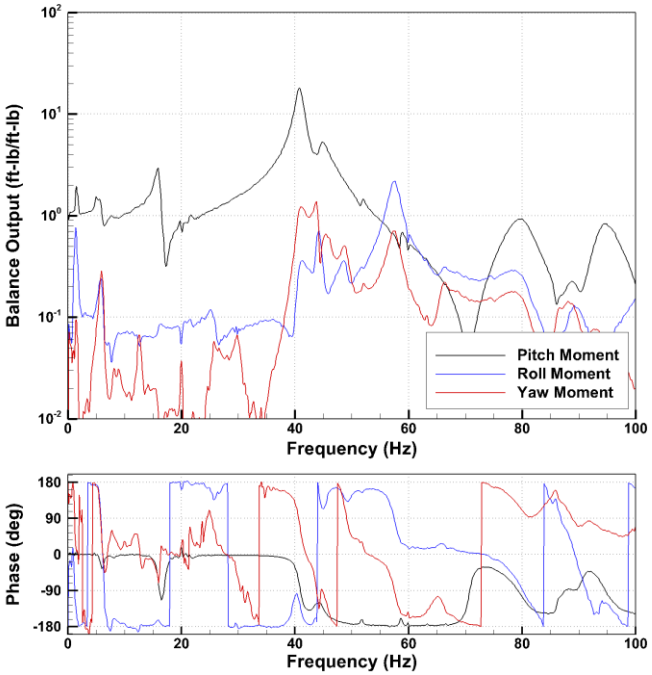

Figure A.11. Balance transformation: Pitch, Roll, and Yaw balance outputs to a hub moment in the Y direction (Pitch).

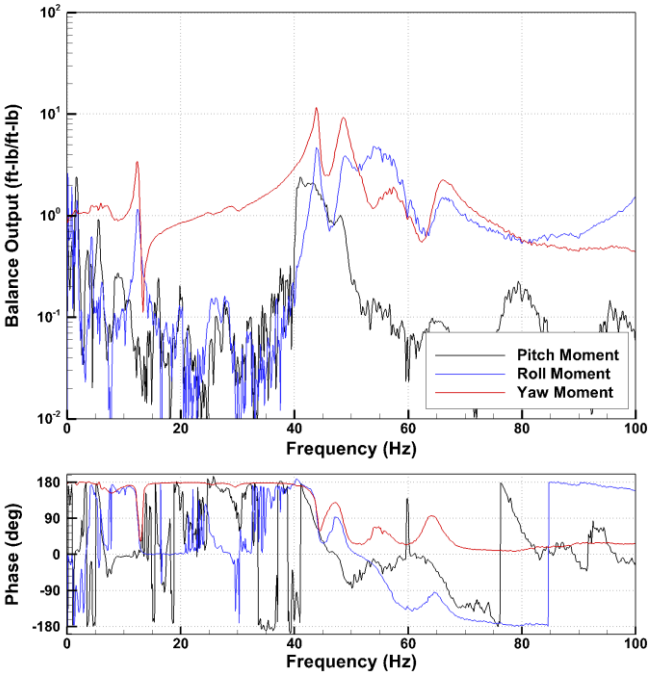

Figure A.12. Balance transformation: Pitch, Roll, and Yaw balance outputs to a hub moment in the Z direction (Yaw).

APPENDIX B: COMPLETE HUB MOTION FREQUENCY RESPONSE

The hub motion frequency response functions are developed from the same vibration tests performed for calculating the balance transfer functions, with a shaker connected at multiple points on the dummy hub and oriented in multiple directions. Each of these tests results in a measured frequency response function (FRF) of four triaxial accelerometer located at the center of each hinge. The accelerometers measure acceleration in 3-degree of freedom (DOF) relative to the applied load at the hub. Depending on the orientation and location of the excitation force, a combination of forces and moments are produced at the center of the hub. The hub was assumed to move as a rigid body with regards to the accelerometer motion, as a result the 6-DOF motion at the center of the hub can be calculated. Thus, having 12 responses at the hub and sufficient independent load directions allow the 6-DOF hub motion FRFs to be resolved from accelerometer FRFs using a method similar to the balance transfer function. The following figures present the balance transformation function which includes 36 components to represent all direct interactions and coupling terms. The first three figures display the linear acceleration as a function of axial force (Fx), side force (Fy), and normal force (Fz).

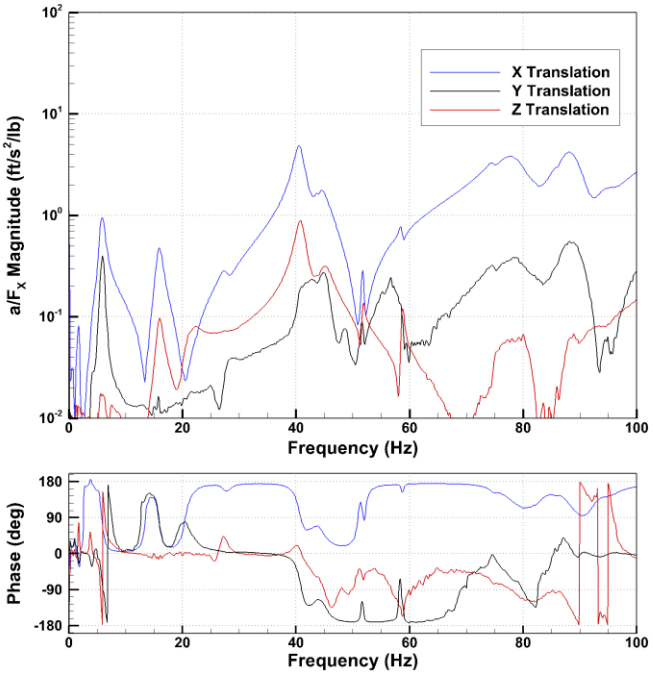

Figure B.1. Hub translational acceleration in X, Y, and Z direction due to a hub force in the X direction (Axial).

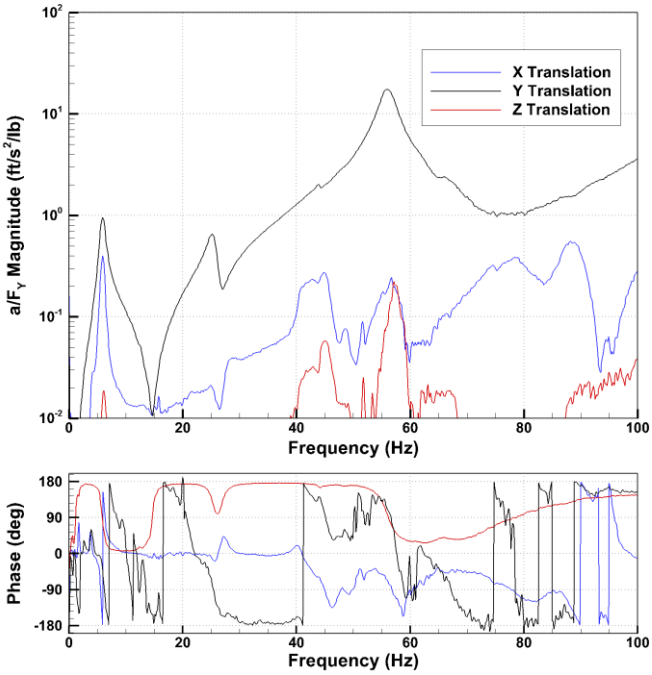

Figure B.2. Hub translational acceleration in X, Y, and Z direction due to a hub force in the Y direction (Side).

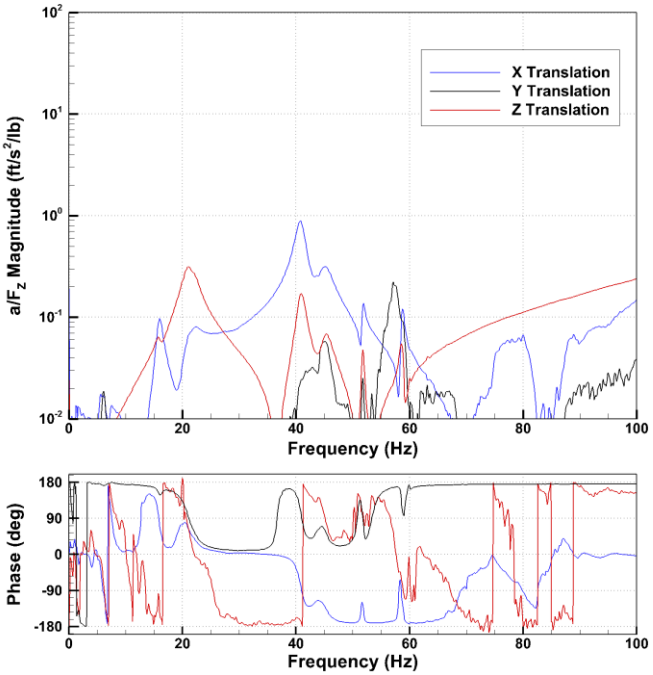

Figure B.3. Hub translational acceleration in X, Y, and Z direction due to a hub force in the Z direction (Normal).

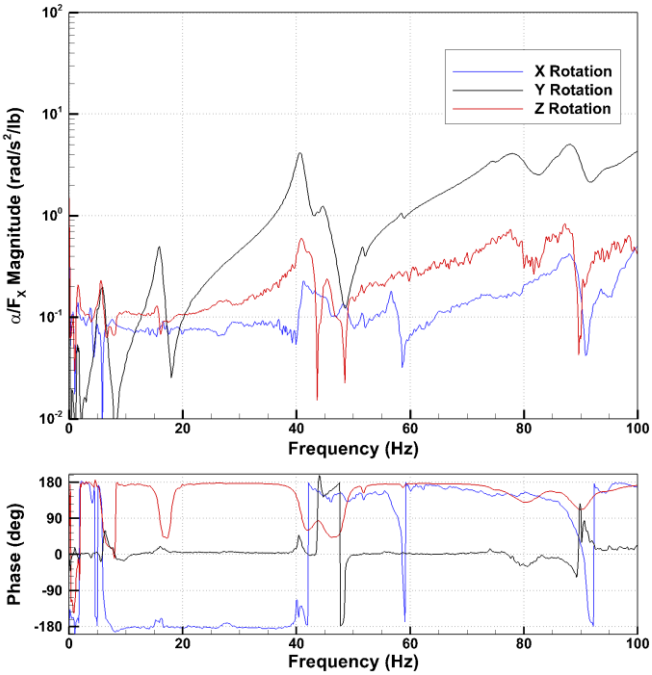

Figure B.4. Hub angular acceleration in X, Y, and Z direction due to a hub force in the X direction (Axial).

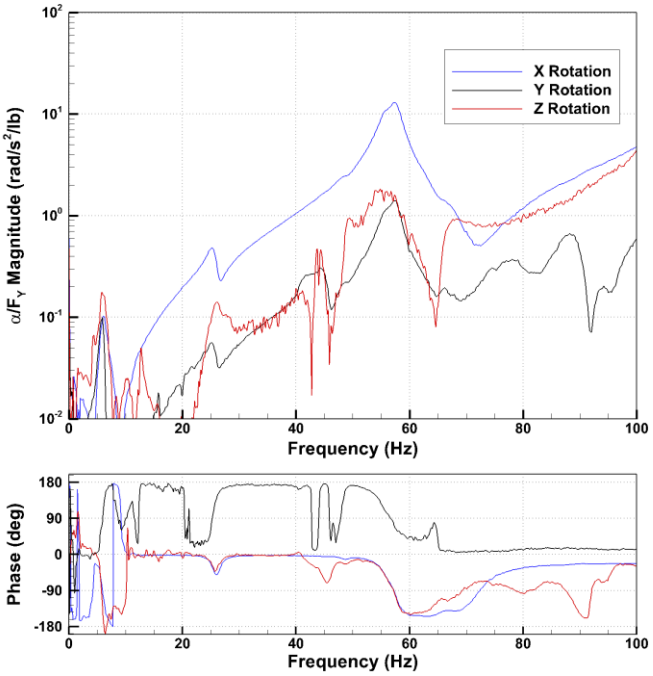

Figure B.5. Hub angular acceleration in X, Y, and Z direction due to a hub force in the Y direction (Side).

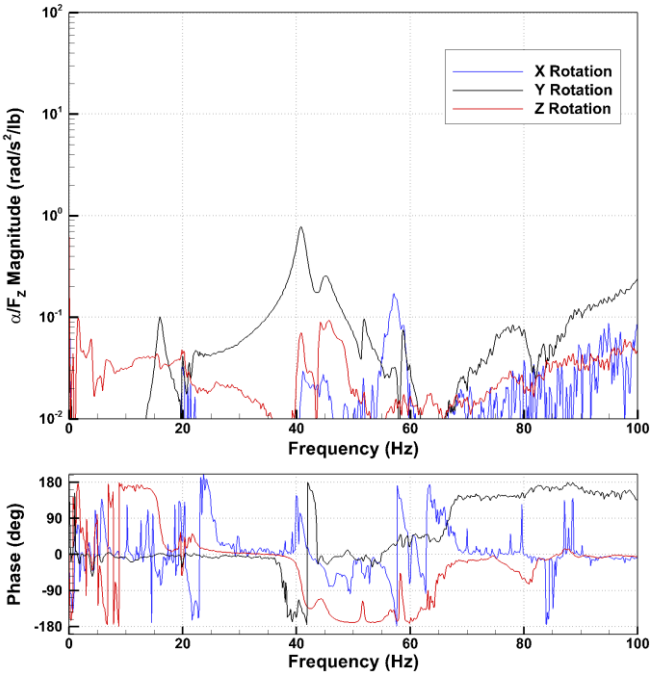

Figure B.6. Hub angular acceleration in X, Y, and Z direction due to a hub force in the Z direction (Normal).

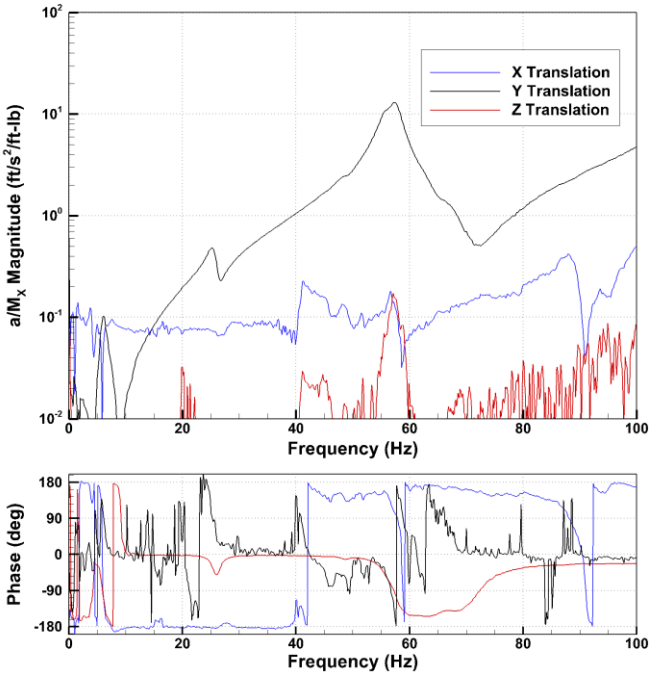

Figure B.7. Hub translational acceleration in X, Y, and Z direction due to a hub moment in the X direction (Pitch).

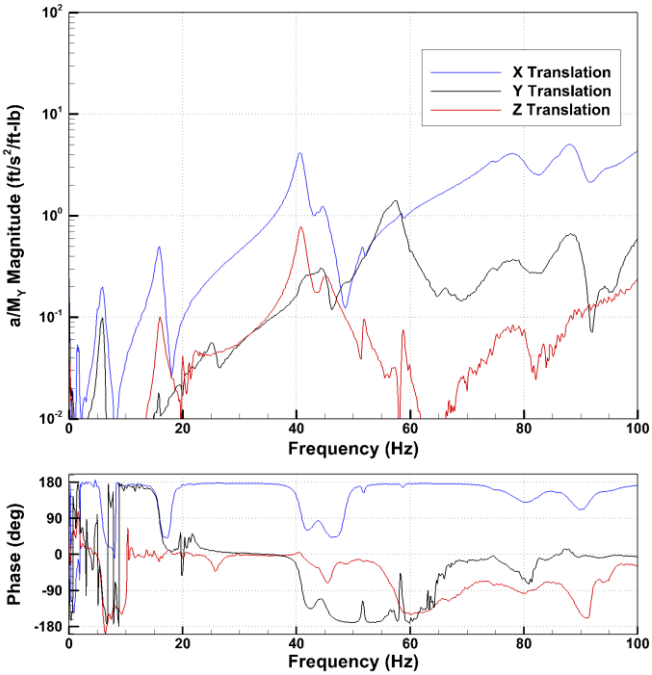

Figure B.8. Hub translational acceleration in X, Y, and Z direction due to a hub moment in the Y direction (Roll).

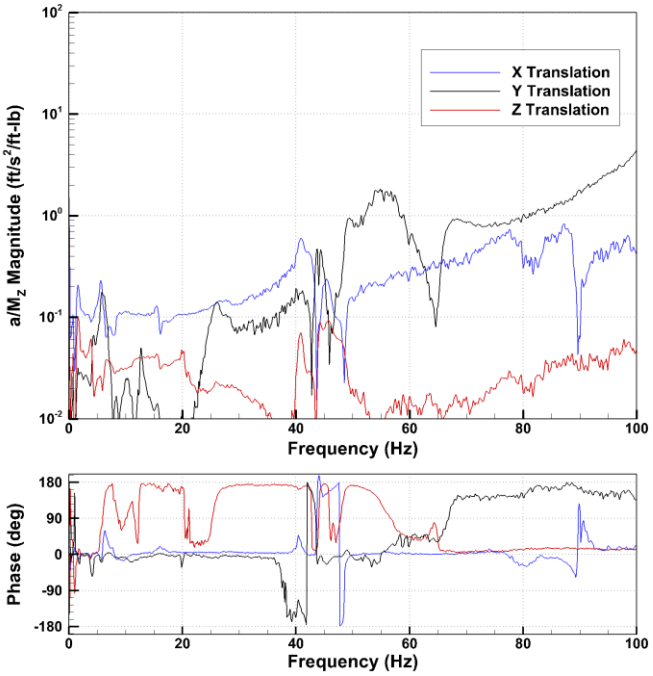

Figure B.9. Hub translational acceleration in X, Y, and Z direction due to a hub moment in the Z direction (Yaw).

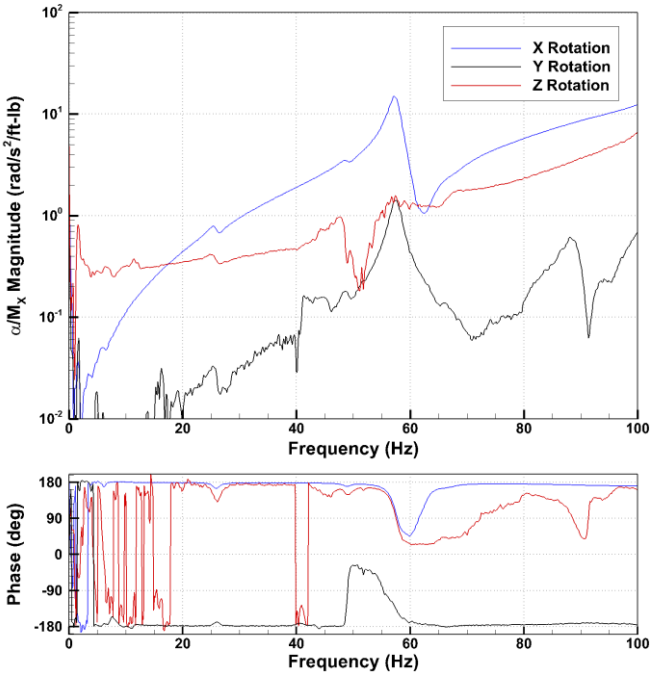

Figure B.10. Hub angular acceleration in X, Y, and Z direction due to a hub moment in the X direction (Pitch).

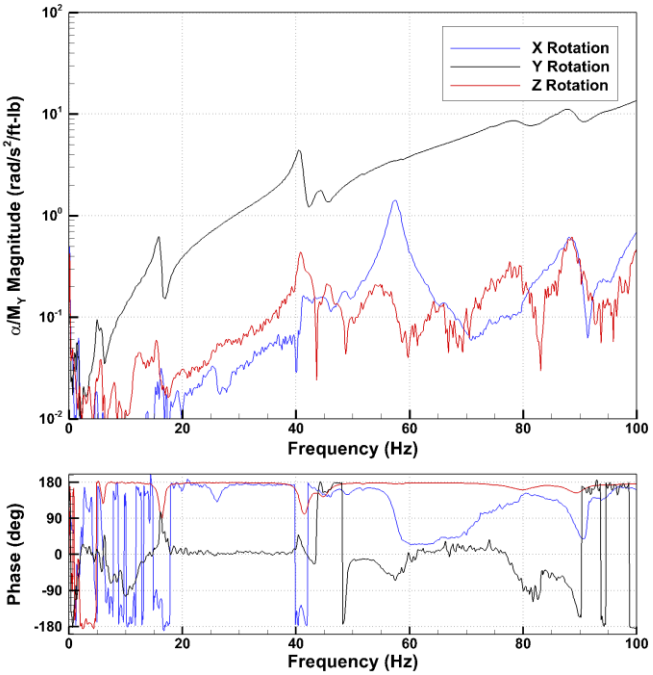

Figure B.11. Hub angular acceleration in X, Y, and Z direction due to a hub moment in the Y direction (Roll).

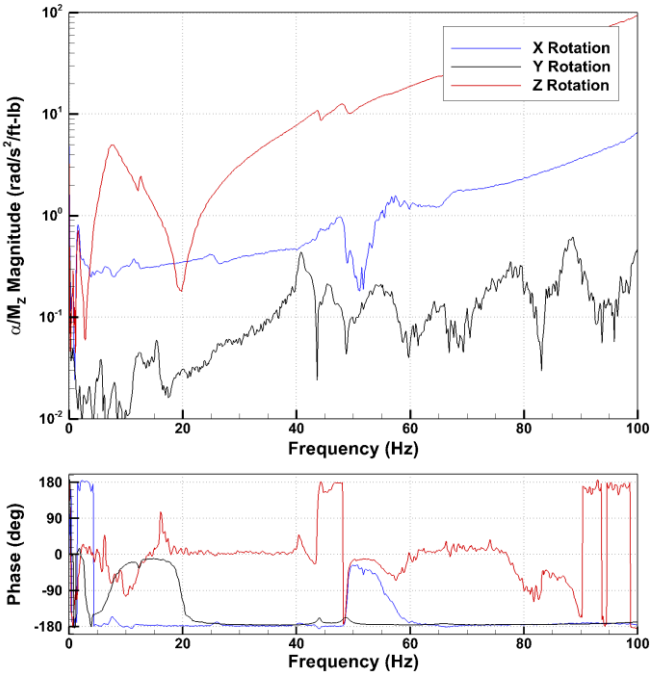

Figure B.12. Hub angular acceleration in X, Y, and Z direction due to a hub moment in the Z direction (Yaw).

REPORT DOCUMENTATION PAGE

Form Approved
OMB No. 0704-0188

1. REPORT DATE *(DD-MM-YYYY)*	2. REPORT TYPE	3. DATES COVERED *(From - To)*
01-03-2017	Technical Memorandum	

4. TITLE AND SUBTITLE

A Dynamic Calibration Method for Experimental and Analytical Hub Load Comparison

5a. CONTRACT NUMBER

5b. GRANT NUMBER

5c. PROGRAM ELEMENT NUMBER

6. AUTHOR(S)

Kreshock, Andrew R.; Thornburgh, Robert P.; Wilbur, Matthew L.

5d. PROJECT NUMBER

5e. TASK NUMBER

5f. WORK UNIT NUMBER

432938.11.01.07.43.40.08

7. PERFORMING ORGANIZATION NAME(S) AND ADDRESS(ES)

NASA Langley Research Center
Hampton, VA 23681-2199

8. PERFORMING ORGANIZATION REPORT NUMBER

L-20736

9. SPONSORING/MONITORING AGENCY NAME(S) AND ADDRESS(ES)

National Aeronautics and Space Administration
Washington, DC 20546-0001

10. SPONSOR/MONITOR'S ACRONYM(S)

NASA

11. SPONSOR/MONITOR'S REPORT NUMBER(S)

NASA-TM-2017-219601

12. DISTRIBUTION/AVAILABILITY STATEMENT

Unclassified
Subject Category 02
Availability: NASA STI Program (757) 864-9658

13. SUPPLEMENTARY NOTES

14. ABSTRACT

This paper presents the results from an ongoing effort to produce improved correlation between analytical hub force and moment prediction and those measured during wind-tunnel testing on the Aeroelastic Rotor Experimental System (ARES), a conventional rotor testbed commonly used at the Langley Transonic Dynamics Tunnel (TDT). A frequency-dependent transformation between loads at the rotor hub and outputs of the testbed balance is produced from frequency response functions measured during vibration testing of the system. The resulting transformation is used as a dynamic calibration of the balance to transform hub loads predicted by comprehensive analysis into predicted balance outputs. In addition to detailing the transformation process, this paper also presents a set of wind-tunnel test cases, with comparisons between the measured balance outputs and transformed predictions from the comprehensive analysis code CAMRAD II. The modal response of the testbed is discussed and compared to a detailed finite-element model. Results reveal that the modal response of the testbed exhibits a number of characteristics that make accurate dynamic balance predictions challenging, even with the use of the balance transformation.

15. SUBJECT TERMS

Aeroelastic; Analysis; Rotor; Transonic dynamics tunnel; Wind tunnel

16. SECURITY CLASSIFICATION OF:			17. LIMITATION OF ABSTRACT	18. NUMBER OF PAGES	19a. NAME OF RESPONSIBLE PERSON
a. REPORT	b. ABSTRACT	c. THIS PAGE			STI Help Desk (email: help@sti.nasa.gov)
U	U	U	UU	31	19b. TELEPHONE NUMBER *(Include area code)* (757) 864-9658